

Advances in Physics: X



ISSN: (Print) (Online) Journal homepage: https://www.tandfonline.com/loi/tapx20

Brighter, faster, stronger: ultrafast scattering of free molecules

Asami Odate, Adam Kirrander, Peter M. Weber & Michael P. Minitti

To cite this article: Asami Odate, Adam Kirrander, Peter M. Weber & Michael P. Minitti (2023) Brighter, faster, stronger: ultrafast scattering of free molecules, Advances in Physics: X, 8:1, 2126796, DOI: 10.1080/23746149.2022.2126796

To link to this article: https://doi.org/10.1080/23746149.2022.2126796





REVIEW

OPEN ACCESS Check for updates



Brighter, faster, stronger: ultrafast scattering of free molecules

Asami Odate^a, Adam Kirrander^b, Peter M. Weber^a and Michael P. Minitti^c

^aDepartment of Chemistry, Brown University, Providence, Rhode Island, USA; ^bDepartment of Chemistry, Physical and Theoretical Chemistry Laboratory, University of Oxford, South Parks Road, Oxford, UK: "SLAC National Accelerator Laboratory, Menlo Park, California, USA

ABSTRACT

Advances in FEL technologies have contributed remarkably to various scientific fields over the past decade, and ultrafast molecular dynamics is no exception. The ability to probe motions of the molecule via scattering provides uniquely direct structural information, which, when combined with traditional spectroscopic techniques of comparable temporal resolution, paints a holistic movie of the molecular dynamics. This review aims to provide an introduction to the ultrafast scattering of gas-phase molecules, and to identify the key results and technological breakthroughs that advance our acquaintance of ultrafast molecular dynamics, with a particular focus on the achievements in ultrafast molecular dynamics since the first generation of FEL facilities. We present a brief history of gas-phase ultrafast scattering and the fundamentals of electron- and x-ray scattering, highlighting the complementarity, differences, and bottlenecks of the two experimental scattering methods. We then consider key upgrades in XRS and UED experiments that facilitated the unprecedented spatiotemporal resolution that enabled many of the notable results in the field. Finally, we examine anticipated facility upgrades that address the demand for experimental versatility and enable further developments and exploration.

ARTICLE HISTORY

Received 1 June 2022 Accepted 9 September 2022

KEYWORDS

FEL & MeV science: scattering & diffraction; gasphase molecular dynamics; structural techniques; XFEL; ultrafast chemistry

CONTACT Michael P. Minitti aminitti@slac.stanford.edu SLAC National Accelerator Laboratory, 2575 Sand Hill Road, M/S 10 Menlo Park, CA, 94025 USA

1 Scope of the review

This review summarizes developments of ultrafast x-ray and electron scattering in the context of gas-phase molecular reaction dynamics. Recent advances greatly benefit from the development of large scale facilities, whose key features are reviewed in Section 5. Section 6 highlights selected results that take full advantage of the new tools available, both in terms of apparatus and data analysis. In the conclusion, we discuss opportunities for further advances and new directions of ultrafast scattering.

2 Motivation to study molecular dynamics by scattering

Rapid advances in light sources around the world have extended the spatial and temporal limits in studies of molecular dynamics. While early experiments of femtosecond-scale chemical dynamics were mostly based on laboratory scale techniques [1], the field has now advanced on the strength of facility-scale instrumentation. Yet the fundamental questions in ultrafast molecular dynamics remain the same – capturing transient intermediate species and events of chemical reactions and to illuminate the overall structural dynamics in a molecular time scale. While traditionally, spectroscopic methods were employed to yield information about the evolution of electronic and vibrational states during chemical reactions, recent advances in x-ray free-electron lasers (XFELs) have enabled the direct measurement of time-dependent molecular structures unaffected by the limitations that the time-energy uncertainty relationship imposes on ultrafast spectral measurements. [2–5].

X-ray and electron scattering are attractive for the study of ultrafast molecular dynamics for several reasons. First, scattering experiments provide direct insight into molecular structures at atomic scales. Additionally, because scattering fundamentally probes electron density distributions, they can observe the time-dependent rearrangements of electronic structure during reactions [6]. The structural information obtained from scattering is complementary to the energy-resolved information offered by spectroscopic methods. Combined, scattering and spectroscopy can paint a holistic picture of the molecular dynamics during photochemical reactions. Modern XFELs deliver the high intensity, high brilliance, and ultrashort pulse durations required for pump-probe experiments on timescales relevant to chemistry. Future developments are expected to yield even brighter and shorter pulses, advancing us towards the eventual goal of capturing transition states of chemical reactions on a single-molecule basis.

Scattering experiments have successfully captured the dynamics of electrocyclic reactions [7, 8], photodissociation [9, 10], coherent vibration motion of excited state molecules [4, 11], and revealed details of transitions

to electronically excited states using the response of electron densities and the transition dipole moments upon excitation [2], all with unprecedented temporal and spatial resolution. These findings were aided and complemented by advances in scattering theory and *ab initio* methods (see Section 6.1), which symbiotically benefited from the experimental result to test the new theories against. As the field of molecular dynamics expands to larger molecular system beyond the small polyatomics studied to date, theoretical methods must improve not only in accuracy but also in computational efficiency.

3 Brief history: ultrafast gas-phase X-Ray Scattering (XRS) and megaelectron-volt ultrafast electron diffraction (MeV-UED)

The measurement of molecular structures of free molecules in the gas phase suffers from low scattering cross-sections, but offers the opportunity to study isolated molecular behaviour free of surrounding environment effects. In 1929, gas-phase x-ray diffraction was first conducted on CCl₄ vapour by Debye et al. whose scattering equation remains widely used to this day [12]. In 1930, Mark and Wierl showed that electron diffraction can reduce the exposure time because the scattering cross-section for electrons are much higher [13]. Throughout the 20th century, many gas phase electron diffraction experiments used continuous electron beams to measure the static, ground state structures of most common small molecules [14].

To follow the dynamics of a molecular reaction including transient events and intermediary species, scattering experiments had to be extended into the time domain. The generation of ultrashort electron pulses was pioneered in the 1980's [15-17]. With 20 keV electron energies and 100 ps pulse durations, electron diffraction at that time was limited by both the spacecharge effect (see Section 4.2) and the spatial and read-out time resolution of the detector, and thus only suitable for picosecond-range structural kinetics studies in solid samples. The next important development was the use of ultrafast laser sources, often at high repetition rates, to generate much shorter pulses [18-22].

At relativistic speeds, the space-charge interactions between electrons in a pulse are minimized, so that it is possible to pack $10^4 - 10^5$ electrons in a single pulse while maintaining ultrashort (120–150 fs) pulse duration [23–25].

Laser-based plasma sources offered an early entry to the time-domain for x-ray diffraction, even though their low brightness limited the samples to solid materials [26-29]. The advent of x ray free electron lasers had a transformative impact on the field. High-gain free-electron lasers (FELs) were initially developed in the 1970–80s [30–32]. The removal of the optical cavities, which previously posed limitations, allowed access to shorter wavelength ranges. The construction of a dedicated x-ray FEL (XFEL) facility was first proposed in 1992 at SLAC [33]. Germany's FLASH became the first operating XFEL in XUV and soft x-ray regime with a peak-brilliance of more than 10²⁸ photons/s/mrad²/mm²/0.1% BW, exceeding the peak-brilliance of the existing synchrotron radiation at the time by several orders of magnitude [34]. In 2009, LCLS became the first hard XFEL (8.3 keV) with a comparable high brilliance to come online. Followed by SACLA in Japan (2011) and FERMI in Italy (2012), these instruments are recognized as first-generation XFEL sources [35, 36].

4 Foundations of X-Ray Scattering (XRS) and UED

The following sections aim to clarify the complimentarity of x-ray and electron scattering and put the temporal and spatial resolution in context. Readers are directed to the original studies cited in the section as well as the references therein for more detailed explanations.

4.1 Fundamental concepts

While the experimental implementation of x-ray and electron scattering is very different, the basic information content of the two experiments are closely related. Ignoring the effects of chemical bonding, the Debye formula describes the scattering signals of a molecule with N atoms as a summation over all pairwise atomic scattering interferences. For x-ray scattering, the total scattering intensity at a detector at distance R is given by

$$I_{total}^{IAM} = \frac{I_0}{R^2} \frac{e^4}{\left(m_e^2 c^4\right)} P(2\theta, \phi) \left(\sum_{i,j}^{N} f_i(q) f_j(q) \frac{\sin(q R_{i,j})}{q R_{i,j}} + \sum_{i=1}^{N} S_{inel,i}(q) \right)$$
(4.1)

where I_0 is the intensity of the incoming radiation and $f_i(q)$ and $S_{(inel,i)}(q)$ are the elastic and inelastic atomic form factors, respectively, for the *ith* atom. The scattering signal scales as the Thomson differential scattering cross section $\frac{e^4}{(m_c^2c^4)}$. The absolute value of the momentum transfer vector is given by $q = |k - k_0| = 2k_0 sin(2\theta)$, where 2θ is the scattering angle. An additional polarization factor $P(2\theta, \varphi)$ needs to be applied for both polarized or unpolarized x-ray beams [37].

The Debye formula is also used for electron scattering, but the momentum transfer is traditionally given the letter s. For non-relativistic electrons, the Rutherford scattering cross section $\frac{4m_e^2c^2}{\hbar^2s^4}$ applies, and according to the Mott-Bethe formula the atomic form factors are given by $(Z_i - f_i(q))$, where Z_i is the nuclear charge of atom i. Electron scattering does not have a polarization factor. Because Rutherford scattering arises from the Coulomb interaction between the electron in the beam and the charges in a molecule, it depends on the charge density of both the electrons and the

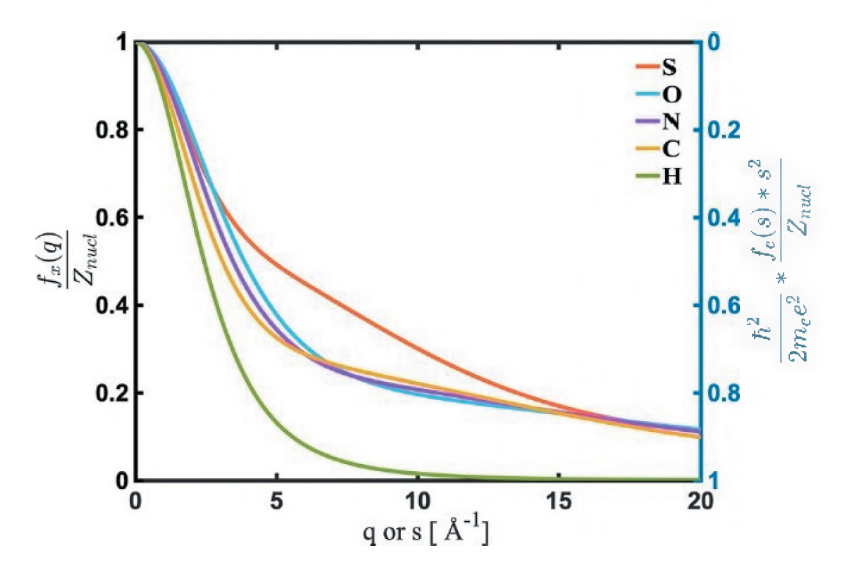


Figure 1. Atomic form factors of sulphur, oxygen, nitrogen, carbon, and hydrogen for x-ray scattering (black vertical axis) and electron scattering (blue vertical axis). Figure from Ref.[38].

nuclei. The Rutherford scattering cross section is much larger than the Thomson cross section, but it is encumbered by the $1/s^4$ term that causes the signal to rapidly decay for scattering vectors of increasing magnitude.

Within the Debye formula and the Mott-Bethe approximation there is little difference in the information content of x-ray and electron scattering. This is illustrated by Figure 1, which shows the complementarity of the x-ray and electron scattering form factors of a selection of atoms [38]. The decrease of the x-ray structure factor with increasing scattering vector is mirrored by an increase of the electron scattering factor, so that a measurement returns similar information, albeit with greater sensitivity to the nuclei in the case of electron scattering [39].

While the Debye formula is widely used, it is well established that it is not sufficient for very accurate measurements. Since the atomic scattering factors are the Fourier transforms of the electron density distributions,

$$f_i(\mathbf{q}) = \int \rho_i(\mathbf{r})e^{i\mathbf{q}\mathbf{r}}d\mathbf{r} \tag{4.2}$$

Electronic excitation of atomic or molecular systems gives rise to effects that have long been predicted [40, 41] and that have more recently been observed in x-ray pump-probe experiments [4, 42], as well as in MeV-UED experiments [23].

4.2 Temporal resolution

An important criterion to assess experimental performance is the temporal resolution. For pump-probe x-ray scattering experiments, it is only limited by the duration of the optical and the x-ray pulses, and by the jitter between them. Modern XFELs can easily achieve pulses in the sub 10–30 fs regime. Instead of relying on a very small jitter, advances in timing measurements allow for shot-by-shot binning of the scattering signals into time bins [43]. For most chemical dynamics experiments, which often use UV pulses to induce the chemical reaction, the duration of the optical pump pulse is therefore the factor that limits the temporal resolution. Progress in the generation of deep UV pulses with durations that match those of the x-ray pulses will be most welcome [44, 45].

For electron scattering experiments, the temporal resolution can be approximated as as [46]

$$\tau = \sqrt{\tau_e^2 + \tau_{ph}^2 + \tau_{TOA}^2 + \tau_{VM}^2}$$
 (4.3)

where τ_e and τ_{ph} are the probe and pump pulse duration, τ_{TOA} is the time-of-arrival jitter, and τ_{VM} is the velocity mismatch. In UED experiments with sub-relativistic electron pulses, space-charge effects often broaden the electron pulse far beyond the duration of the typical optical pulses. The velocity mismatch between the pump (laser) and probe (electron beam) is also significant in keV UED experiments. Tilting the optical laser pulse front was proposed as a solution to push the temporal resolution to several hundred fs,[47–49] which combined with dc-rf keV electron gun, was able to achieve temporal resolution of 240 fs [50].

The development of MeV electron beams along with radio frequency cavities to compress the electron bunches at the interaction region has significantly improved the temporal resolution for UED experiments [51– 53]. Since space-charge repulsion scale as $1/(\beta^2 \gamma^3)$ where β^2 , is the ratio of the electron velocity over speed of light, and $\gamma = 1/\sqrt{1-\beta^2}$, the effect can be minimized dramatically in MeV regime while sustaining a high number of electron per pulse. This results in an improved pulse charge density by a factor of $10^3 - 10^4$ compared to 100 keV systems at comparable repetition rate. It is noted that table-top, keV source with similar charge density at 100 fs has been demonstrated previously [48]. However, the RF buncher does not come with- out a cost, since the RF phase jitter can cause τ_{TOA} to be larger than 100 fs [54]. Today, SLAC's MeV-UED can produce ≈150 fs pulse of up to 100 fC (10^4 – 10^6 electrons). Considerable effort to shorten the pulse duration to sub-100 fs has been hindered by the timing jitter and the RF phase correction required for every shot. Since the jitter correction technique is limited by the detector response time, this option is only practical for

low repetition rate experiments. This may ultimately become a concern given that gas-phase UED, which suffer from high noise levels, require many shots (and therefore as many jitter correction) to reveal the chemical dynamics. It is noted that for both XRS and UED, the increasing repetition rate is only beneficial when coupled with improvement in real time data analysis infrastructure [55] that allows timely decision making during the limited beam time.

4.3 Spatial resolution

In principle, the spatial resolution of a static scattering experiment is limited by the wavelength of the probing beam, requiring a sub-Å light source with sufficient brightness. In practice, this is further limited by the accuracy of the measurement of the scattering intensity, I(a). In the 20th century, methods have been developed for extracting molecular structures from conventional gas-phase electron diffraction data. With vastly larger electron currents (up to μA) than possible in pulsed UED instruments, measurements went to very large scattering vectors, often $>30 \text{ Å}^{-1}$. Using rotating sectors to provide a scattering angle dependent attenuation, photographic plates and analog readouts of the gray scales, quantitative measurements were difficult to attain. Researchers separated 'atomic scattering' (the i = j terms in Equation 4.4) from 'molecular scattering' (the $i \neq j$ terms) by fitting a background through the points where the latter terms are zero. This results in a pleasing oscillatory curve, often expressed as,

$$sM(s) = \frac{I_{mol}(s)}{I_{atom}(s)} \tag{4.4}$$

but one notices that the structure that is to be measured needs to be known or assumed in order to separate the atomic from the molecular scattering. Nevertheless, given the very large range of scattering vectors accessible to those traditional instruments, excellent molecular structures were obtained with accuracies of atom-atom distances in the milli-Ångstrom range [14].

Aided by tremendously sensitive detectors with wide dynamic range, but employing pulsed electron or photon beams that give rise to much weaker scattered signals, the situation today is dramatically different. Measurements routinely reach the shot noise limit, making it possible to detect the very small changes in the signal induced by laser excitation. The experiments indeed measure the changes in the molecular structures, i.e. the difference between the time-dependent excited structure and the static ground state structure. The latter can either be measured in the course of the experiment, or calculated with high level computational methods.

The objective of a scattering experiment is to determine a molecular structure, implying that for a N-atomic molecule, 3N-6 coordinates have to be measured. A direct inversion of a one-dimensional scattering pattern into a three-dimensional structure is, however, impossible without further assumptions. Even though widely published, pair distribution functions (obtained by transforming the sM(s) patterns) do not reveal structures for all but the smallest and most symmetric molecules. It is also a widely held misconception that the way to improve the determination of the molecular structures inevitably necessitates measuring to larger scattering angles. In fact, the noise of the measurement is just as important. While electron scattering experiments often can access a large range of scattering vectors, this is balanced by the often better noise performance of x-ray scattering experiments (see Section 4). In both experiments, sample densities are limited by the absorption of the optical laser pulses, so that improvements must arise either from packing more electrons/x-ray photons into each pulse, or from increasing the repetition rate of the instruments. The latter seems to be the most promising route at the present time.

While direct inversion of pump-probe scattering signals are not possible, methods have been developed to extract highly precise structures of molecules in excited and dynamic states (Figure 3). Standard computational methods are employed to create a large number of molecular structures and for each the scattering pattern is calculated. A comparison with the experimental x-ray scattering data yields, via a plot of the structural parameter versus the deviation, complete molecular structures that are

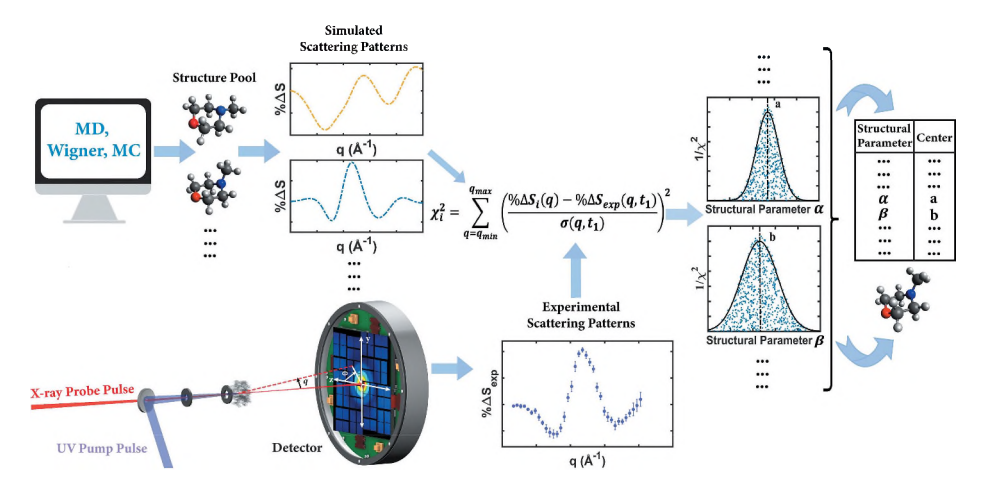


Figure 2. Analysis flow of a typical XRS experiment taken from [56]. First, the structure pool that contains the expansive and dense, energetically viable structures in the vicinity of target structures are generated. The scattering pattern data is then compared parametrically (interatomic distances, bond angles, torsional angles etc.) with the simulated scattering pattern from the structure pool to extract the structure.

inherently self-consistent [6, 56, 57]. Importantly, as the changes in the scattering signals upon laser excitation are observed, the resulting excited state structures are referenced to the ground state structures. This makes it possible to determine excited state structures with a precision approaching that of conventional electron diffraction. While the method was developed for x-ray scattering (Figure 2), it should be equally applicable to pumpprobe electron scattering.

4.4 Comparative evaluation

Despite the complementary nature of x-ray and electron scattering, there are no experimental reports of their relative performance given current instrumentation. However, such measurements are underway and will without doubt be very informative. Meanwhile, recent comparative simulations using N-methyl morpholine (NMM) by Ma et al. and ab initio calculation based on ethylene molecule by Stefanou et al. provide some insights by subjecting the scattering signals from x-ray and electron diffraction to comparable data analysis methods in order to illustrate the different strengths between the two techniques [38, 39].

Ma et al. investigated 1) observed scattering signal, 2) noise level, and 3) dynamic structure determination to assess the robustness of electron vs. x-ray diffraction experiments based on the instrument parameters from SLAC National Laboratory. The results showed that despite the fundamentally larger (by a factor of up to 10⁵) cross section of electron scattering over the x-ray scattering, higher probing particle counts per pulse in x-ray beam $(10^{12} \text{ photons/pulse vs. } 3.7 \times 10^4 \text{ e}^{-/\text{pulse in an electron beam})}$ delivers unparalleled performance with regards to noise level reduction and the structure determination as seen in Figure 3. Meanwhile, the MeV instrument of the same repetition rate suffers from large noise level for $s > 8 \text{ Å}^{-1}$ range, inherent to the $1/s^4$ dependence in Rutherford scattering intensity.

The authors compared the fidelity of structure determination by using the method described elsewhere [4]. This method takes advantage of nearly noiseless signal from x-ray diffraction, which compensates for the lack of q-range in the actual experiment (the photon energy in LCLS has since improved from 9.5 keV to maximum of 25 keV, thus expanding the q-range to around 12.6 Å⁻¹). Interestingly, Ma et al. shows that including higher q-range data points, which are inherently noisier than low q-range signal [58] does not necessarily aid in the structure determination using the structure pool method outlined in Ref.[4], but in fact can compromise it unless more probing photons are captured to reduce noise to the level comparable to low q-range.

Both the studies by Ma et al. and Stefanou et al. showed higher sensitivity towards hydrogen atoms for electron diffraction, and in the latter case this is

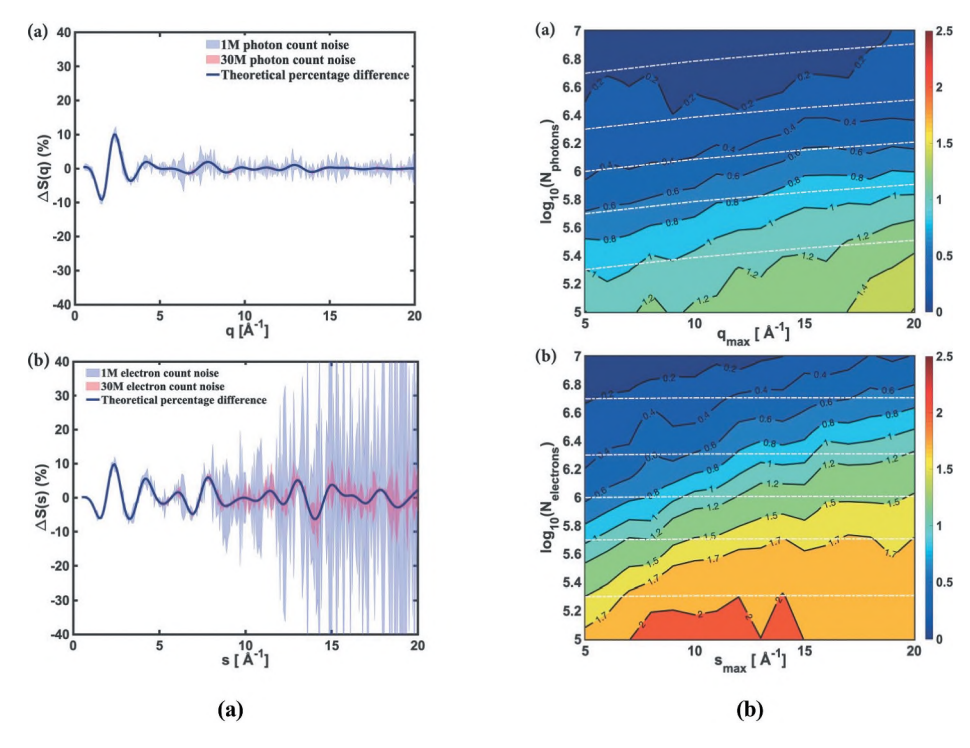


Figure 3. (a) Comparing fractional difference in signals (black) of XRS vs. UED under real experiment condition, assuming 100% excitation. The noise level is calculated based on 1 M photon count noise (purple), and 30 M photon count noise (pink). XRS is virtually noiseless for the qrange accessible by the experiment in both photon count simulations, while UED exhibits strong increase in noise beyond s>8 Å $^{-1}$ (typical experiment accesses up to s=12 Å $^{-1}$), even with the 30 M simulation. (b) Structure determination comparison between XRS vs. UED. The accuracy is depicted such that blue hues indicate higher accuracy. The white dashed lines indicate the number of probing photons required. This shows that while both XRS and UED benefit from having more probe particles, inclusion or a larger momentum transfer range is less critical for XRS than UED.

consistent with the known dynamics of ethylene molecules, where the longer time point dynamics are dominated by hydrogen motion. In theory, electron diffraction is a more suitable technique for observing hydrogen motion assuming that low noise data is available in the high *s*-range. The same trend was found to be true for methyl group rotation motion. It must be emphasised that there are other structure retrieval methods and thus, strictly speaking, the comparative evaluation performed here is based on the Wigner-distributed structural pool generation [11, 50, 59, 60]. The limitations from noise to the structure determination should still be applicable regardless of the specific method used. It is evident that x-ray and electron diffraction can provide complementary information while each may be more sensitive to different aspects of the experiment: the temporal resolution and overall SNR are advantageous in x-ray experiments, while electron diffraction has fundamentally higher scattering cross section that might

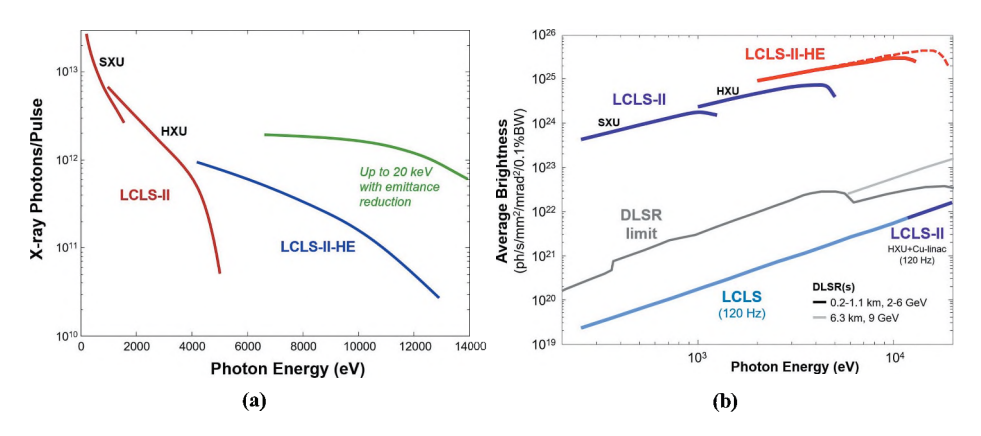


Figure 4. (a) X-ray photons per pulse, calculated for high rep-rate operation from LCLS-II soft x-ray (SXU) and hard x-ray (HXU) at 4 GeV compared with planned upgrade, LCLS-II-HE. (b) Averaged spectral brightness of LCLS, LCLS-II (current) and LCLS-II-HE (planned upgrade). Figures from [61].

enable a more sensitive measurement of smaller atoms. Advances in FEL technology towards brighter pulses and higher repetition rate are un-doubtedly going to benefit both techniques.

5 State-of-the-art apparatus and techniques

The recent advances in gas-phase ultrafast scattering at SLAC were enabled by major upgrades in new and existing facilities as shown in Figure 4. The fourth generation light sources are advancing towards superconducting accelerators (except European XFEL and FLASH that already have this technology), kHz repetition rate, and higher peak brilliance as summarized in Table 1 along with planned timeline and specifications. This section surveys some notable new technology that contributes in this quest, as the light sources around the world undertake large-scale upgrades. For the advances of FEL physics that would impact both the UED and XRS, readers are directed to other sources and the references therein for further information [62–66].

The most remarkable upgrade in UED experiment was the implementation of radio frequency (rf) photoinjectors. A typical accelerating field in an rf gun exceeds 100 MV/m, which is significantly greater than 10–25 MV/m in DC sources. This enables the electrons to reach relativistic speed within a few millimeters, at which point the space-charge effect is minimized while the brightness of electrons are preserved. Additionally, rf electron beams have minimal velocity spread, which also solves the velocity mismatch problem between the optical laser pump and the electron beam probe [46].

Since the first sub-picoseconds MeV UED demonstration by Hastings et al. in 2006 [51], further efforts towards improving bunch compression,

Table 1. Key parameters of the various XFEL (updated from [67]) facilities around the world.

| Country | Facility Name | Photon energy range (keV) | X-Ray pulse energy (a) (mJ) | X-Ray pulse length (b) (fs) | Repetition rate (Hz) | Start date |
|-------------|---------------|------------------------------|--------------------------------|--------------------------------|-------------------------|---------------|
| Germany | FLASH 1 | 0.02-0.03 | 0.01-0.5 | 30-200 | (1-800) x 10 (c) | 2005 |
| | FLASH 2 | 0.01-0.03 | 0.01-1 | 10-200 | (1-800) x 10 | 2016 |
| Italy | FERMI-FEL-1 | 0.01-0.06 | 0.08-0.2 | 40-90 | 10 (50) | 2010 |
| , | FERMI-FEL-2 | 0.06-0.3 | 0.01-0.1 | 20-50 | 10 (50) | 2012 |
| Japan | SACLA BL 2,3 | 4-20 | 0.1-1 | 2-10 | 60 | 2011 |
| | SACLA BL 1 | 0.04-0.15 | 0.1 | 60 | 60 | 2015 |
| Korea | PAL-XFEL | 2.5-15 | 0.8-1.5 | 5-50 | 60 | 2016 |
| | | 0.25-1.2 | 0.2 | 5-50 | 60 | 2016 |
| Switerzland | SwissFEL | 1.8-12.4 | 1 | 10 – 70 | 100 | 2017 |
| | | 0.2-2 | 1 | 10-70 | 100 | 2021 |
| Europe | XFEL-SASE 1,2 | 3-25 | 2 | 10 - 100 | 2700 x 10 (d) | 2017 |
| • | XFEL-SASE 3 | 0.2-3 | 2 | 10-100 | 2700 x 10 | 2017 |
| United | LCLS | 0.3-12 | 2-4 | 2-500 | 120 | 2009 |
| States | LCLS-II | 1 – 25 | 2-4 | 10-100 | 120 | 2021 |
| | | 0.2-5 | 0.02-1 | 10-200 | 10^{6} | 2023 |
| | LCLS-II-HE | 0.2-13 | 0.02-1 | 10-200 | 10^{6} | 2026 |
| | | | | | | (e) |

⁽a): Estimated pulse energy, particularly for projects that are currently under construction at the time of this review.

⁽e): Projected completion date for LCLS-II-HE.

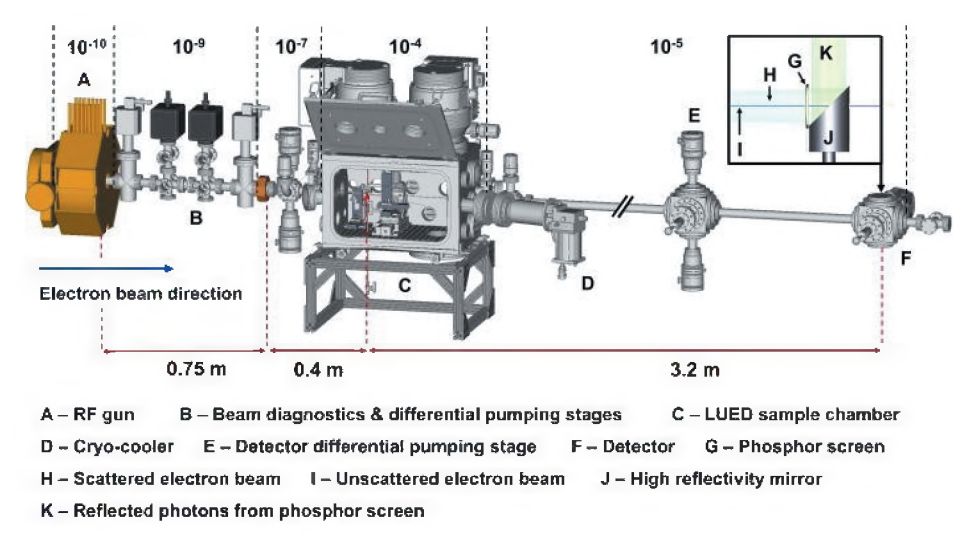


Figure 5. Gas-phase MeV-UED instrument at SLAC. Figure from [68].

timing systems, machine stability, and spatial resolution have culminated in today's robust MeV instrument at SLAC as depicted in Figure 5 [69–71]. Availability of 2–4 MeV electrons at 120 Hz repetition rate and packing 1–100 fC charge per pulse, MeV-UED is complimentary to the XRS experiments. In theory, MeV-UED is a great tool for gas-phase scattering experiment as well, even though the inherent SNR issue along with requirement for sub-100 fs pulses limit the systems of interest. At the moment of this

⁽b): Estimated FWHM of X-ray pulse length based on electron bunch length measurement or designed range.

⁽c): Burst mode operation at 10 Hz, with each macropulse providing up to 800 bunches at 1 MHz.

⁽d): Pulsed mode operation at 10 Hz, with each macropulse providing up to 2700 bunches at 5 MHz.

| Table 2. Key parameters of the variou | s MeV-UED facilities around the world. |
|---------------------------------------|--|
|---------------------------------------|--|

| Country | Facility Name | Electron beam energy range (MeV) | Charge per pulse (fC) | Electrons per pulse | Bunch length (fs) | Repetition rate (Hz) | Start date |
|---------|---------------|--|--------------------------|-----------------------------------|----------------------|-------------------------|---------------|
| Germany | DESY – REGAE | 2–5 | <100 - 1000 | $10^4 - 10^6$ | 7–30 | 50 | 2011 |
| China | Tsinghua | 2-4 | $10^4 - 10^5$ | $10^8 - 10^9$ | 1000-3000 | 5-10 | 2013 |
| | Thomson | | | | | | |
| | scattering | | | | | | |
| | X-ray source | | | | | | |
| | (TTX*) | | | | | | |
| | SHINE*** | 0.75 | 1000-10 ⁴ | 10 ⁸ – 10 ⁹ | 1000 | 10 ⁶ | 2025 |
| United | SLAC MeV-UED | 2-4 | 1-100 | $10^4 - 10^6$ | <150*** | 1-360 | 2014 |
| States | SLAC MeV-UED | 2-3 | 1-100 | $10^4 - 10^6$ | <150*·*·* | 1000 | 2023 |

^{*}https://indico.cern.ch/event/577.810/contributions/2.479.863/attachments/1.424.734/2.185.126/2017-CLIC WS-Thomson_Scattering_X-ray_Source_at_Tsinghua_University.pdf

review, the opportunities for condensed matter MeV-UED appear very promising. Current capabilities and planned future upgrades for various MeV-UED facilities across the globe can be seen in Table 2.

5.1 SASE to seeded

The self-amplified spontaneous emission (SASE) mode has been the standard mode of operation of x-ray FEL[72, 73]. For SASE operation, the x-ray generation starts with the initial shot noise (random electron bunching intrinsic to the electron beam current). Maximum coherence is achieved when the slippage length-velocity mismatch between the electrons and the radiation, is comparable to the electron bunch length (Figure 6). However, the initiating shot noise causes poor longitudinal coherence in SASE pulses [74, 75]. Methods such as low-charge operation (reduces electron bunch length), emittance spoiler [76], and tilted wavefront (both disperses the energetically chirped beam) have improved the longitudinal coherence with some success [77].

While seeded FEL is not immediately beneficial to the gas-phase experiments, it warrants a mention as a trend for the next upgrade of the FEL facilities. A variety of alternative seeding mechanisms has been developed and adopted to the latest XFELs in order to overcome the poor temporal coherence at saturation as well as shot-to-shot stability of the SASE pulses. Many of the seeding mechanism below are in the process of, or will be incorporated in the new generation of FEL facilities. Self-seeding schemes for both hard [78] and soft [80] x-rays have been successfully demonstrated, thus expanding applications ranging from biology [81-83] to materials under extreme condition [84-86].

^{**}http://linac2018.vrws.de/talks/mo2a01_talk.pdf

^{***}Beam charge dependent

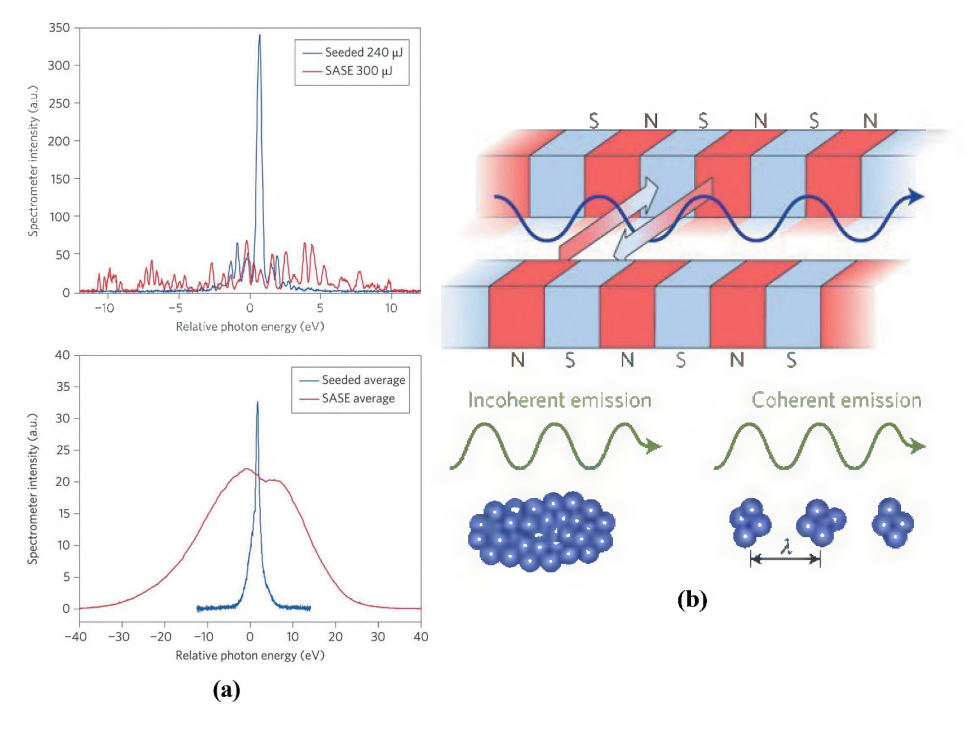


Figure 6. (a) Difference between SASE pulse and seeded pulse for single-shot (top) and averaged over 20,000 shots (bottom), figure from [78]. (b) SASE pulse generation in XFEL, figure from [79].

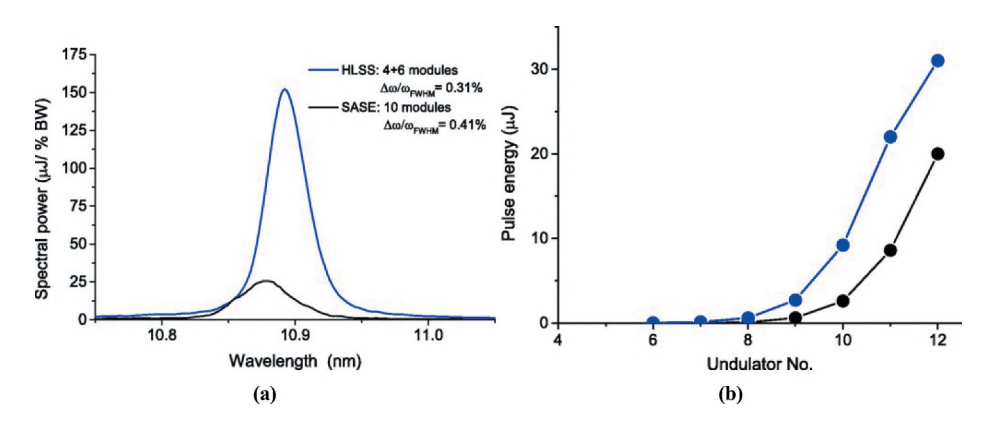


Figure 7. Comparison between HLSS FEL (blue) and SASE FEL (black). (a) Spectral density of the radiation energy with four undulator modules at 33 nm followed by six modules tuned to 11 nm for HLSS FEL, and ten undulator modules for SASE FEL. (b) Pulse energy vs. undulator length. Because HLSS reaches saturation more quickly, the post-saturation tapering is more effective for HLSS (18 μJ to 31 μJ) than SASE (15 μJ to 20 $\mu J J$. Figure from [88].

The self-seeded scheme is a two-step mechanism where the x-rays from the first part of the undulator series is filtered and then used to seed the later part of the undulator after temporally overlapping with the electron bunch (also from the first half of undulators) to generate narrow bandwidth pulse

[67, 87]. The harmonic lasing self-seeding (HLSS) scheme is an example that is already being adopted at FLASH [88]. The main advantage of HLSS scheme is the shorter distance required to reach saturation than SASE operation (Figure 7(b)), while also improving the brightness by a factor of up to 6 [89]. HLSS can be integrated in the CW operation with appropriate undulator design to accommodate this technique. Combined with postsaturation tapering, HLSS can improve the FEL peak power into TW range [87, 90-92]. The relative ease of implementation makes HLSS a promising candidate as the standard operation mode for the next generation of FEL facilities, although the issues stemming from low seed beam power and power fluctuation must be addressed [93].

External seeding is another approach to improve the temporal coherence of SASE pulses. High-gain harmonic generation (HGHG), the most extensively studied external seeding mechanism, was first installed at FERMI with FEL wavelengths ranging from 4-110 nm depending on the single- or double-cascade mode [94, 95]. Instead of initiating the FEL amplification process with shot noise as in the SASE mode, the properties of the external seed beam can be imparted upon the beam, resulting in fully coherent XFEL pulse at a wavelength that is a harmonic of the seed beam. Along with the improved longitudinal coherence, HGHG allows for more stable output spectra, narrower bandwidth, and improved wavelength stability. However, the HGHG design is limited by the power requirement and the repetition rate of the seed beam and the low frequency up-conversion starting from a UV seed [96, 97]. Some variations of the HGHG scheme [96, 98] are being explored to address the issue and to make HGHG compatible with harder x-rays and higher repetition rates. Experimental and theoretical comparisons of seeded vs. unseeded FEL have been reported previously in [99, 100] and the references therein.

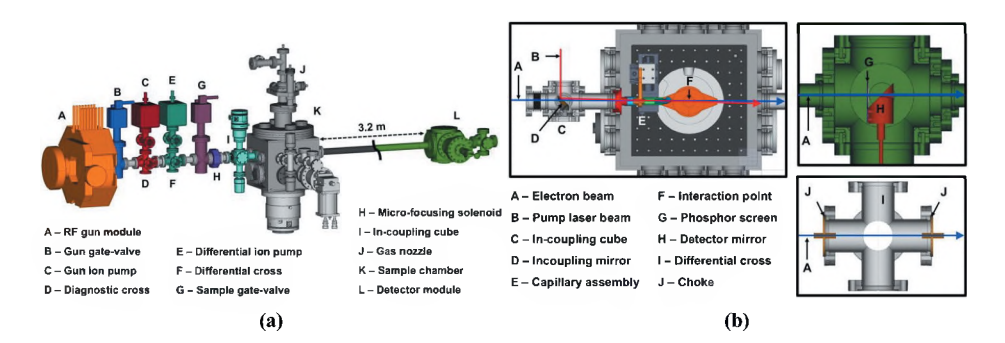


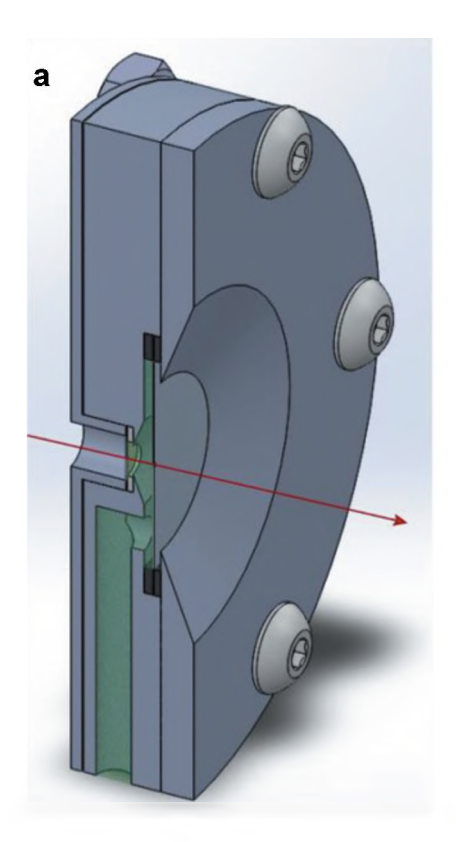
Figure 8. MeV-UED instrument at SLAC. Figure from [53].

5.2 Sample delivery methods

The success of gas-phase UED and XRS hinges not only on the pumpingand probing beams but also the sample delivery. The technical details of for MeV-UED cell [53] and XRS cell [37] used at SLAC National Laboratory are found in respective reports and the references therein.

The MeV-UED sample chamber as shown in Figure 8(b) houses a 3D translation stage to optimize the position of the sample nozzle, and the users have the choice to deliver the sample with continuous flow cell or a heated pulsed nozzle. The excess sample is immediately condensed onto the cryocooled cold trap underneath the interaction region. The scattered electron is detected on a phosphorus screen, 3.2 m downstream of the interaction region. A tapered hole at the center of this screen and the subsequent detector mirror is carefully designed to minimize stray laser light while also allowing the undiffracted beam to pass without saturating the detector. This has reduced the background diffration pattern casued by the laser significantly.

In the gas-phase XRS experiment, the optimization of the distance between the scattering cell and the detector is a critical step to maximize the spatial resolution and the overall signal level. The sample cell (Figure 9)



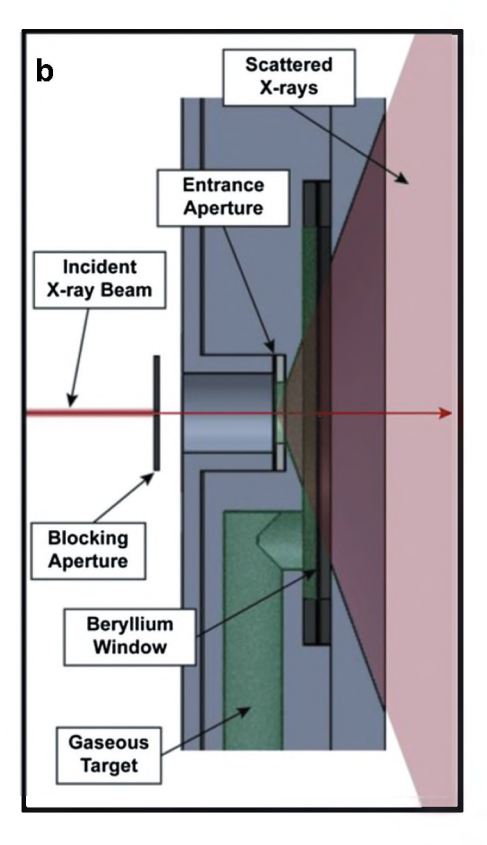


Figure 9. Cross section of the x-ray scattering cell as described in [37].



was designed with consideration to minimize scattering of the primary x-ray beam by apparatus components, while ensuring sufficient sample flow and beam path clearance. The x-ray enters from windowless entrance and exits through a hole in a 100 µm-thin berylium window after the 2.4 mm interaction region. The short pathlength minimizes the Beer-Lambert attenuation of the UV pump pulse, while also avoiding unwanted multiphoton interaction. Additionally, the short interaction region enables good resolution of the scattering angle. With every detector upgrade and the sample delivery requirement (e.g. pulsed molecular beam), a careful re-design of gas cell is essential.

6 Select recent results

The first successful recording of a gas-phase molecular reaction by Minitti et al. (Figure 10) in 2015 inspired studies of molecular dynamics across many different molecular systems as well as technical improvements in both x-ray and electron diffraction experiments [7, 101–104]. The prototypical electrocyclic reaction of cyclohexadiene-moiety is at the core of photoinduced synthetic chemistry, molecular switch technology, as well as biologically important molecules such as vitamin D. The ring-opening reaction of 1,3-cyclohexadiene to 1,3,5-hexatriene upon excitation with 267 nm was captured with an unprecedented 25 fs time resolution. Trajectory calculations using abinitio electronic structure methods proved essential in understanding the the overall dynamics and were in excellent agreement with the experimental results. This experiment demonstrated the robustness of XRS as a tool to obtain direct structural information on chemically relevant timescales.

While significant advances have also been made in condensed matter systems [68, 105–109], the following section discusses select recent studies that point toward future directions of gas-phase scattering experiments.

6.1 Recent advances in gas-phase XRS

Capturing excited state structures directly from experiments has been a long standing goal for ultrafast chemistry. Stankus et al. were the first to observe the coherence and dephasing of vibrational motion of polyatomic molecules in real time using gas-phase x-ray scattering [4]. N-methylmorpholine (NMM) was known spectroscopically to have a coherent vibrational motion that survives a nonradiative transition [110], and this motion was captured using ultrafast XRS (Figure 11). All structural parameters, including the amplitude of planarization of amine group as well as changes in every torsional angle of the molecule, were identified with 50 fs time increments.

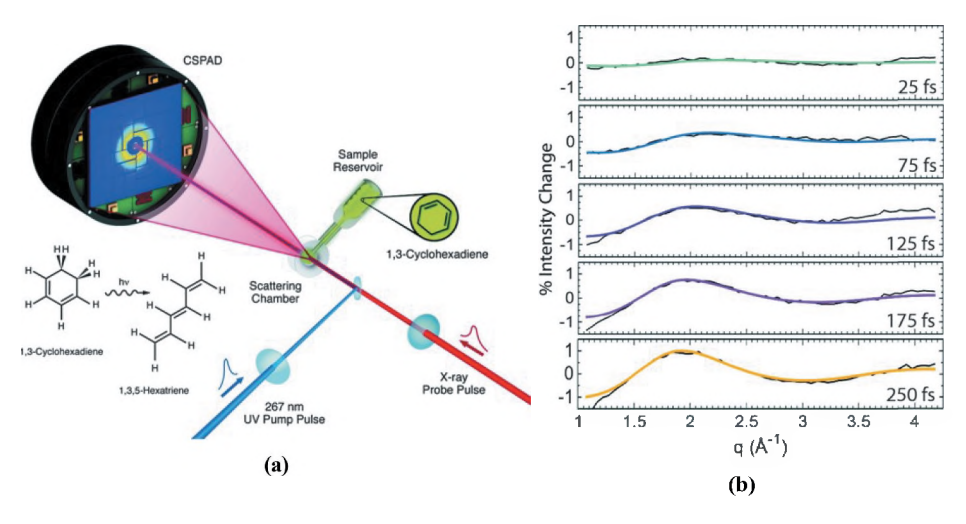


Figure 10. (a) Experimental setup of [7] conducted at LCLS. (b) Experimental scattering signal at specific time delays (black) overlayed with calculated trajectories (colored).

A distinct advantage of pump-probe XRS experiment over spectroscopic methods is the unambiguous assignment of the initial excited states. Traditional spectroscopic tools may leave assignments ambiguous for reasons such as broadening of transitions due to experimental parameters or the inherent linewidths. In XRS, it is possible to isolate the anisotropic contribution to the scattering signal in order to gain more information about the nature of the interaction. This is particularly useful when the reaction involves multiphoton absorption, resulting in a mixture of various excited states, as Natan et al. showed for molecular iodine [10]. In 2018, Yong et al. used the anisotropy to determine the orientation of the transition dipole moment (TDM) of NMM excited to Rydberg states. Different Rydberg state excitations lead to markedly different XRS patterns, and they found that only the transition to the $3p_z$ Rydberg state is consistent with the observed scattering signals [2].

In a further study, Yong et al. investigated the intramolecular charge transfer in *N-N*'-dimethyl-piparazine and were able to experimentally separate two excited state scattering structures (Figure 12) which were determined using the method described in Stankus et al. [37, 42]. The charge delocalization is associated with an increase of the C-C bond distance and a reorientation of the methyl group. From the anisotropic component of the scattering signal it was also possible to determine the vector alignment of the transition dipole moment as described in [42]. Finally, it was possible to determine the time constant of the charge redistribution reaction as 3.0 ps, which is in excellent agreement to previous spectroscopic experiments [111].

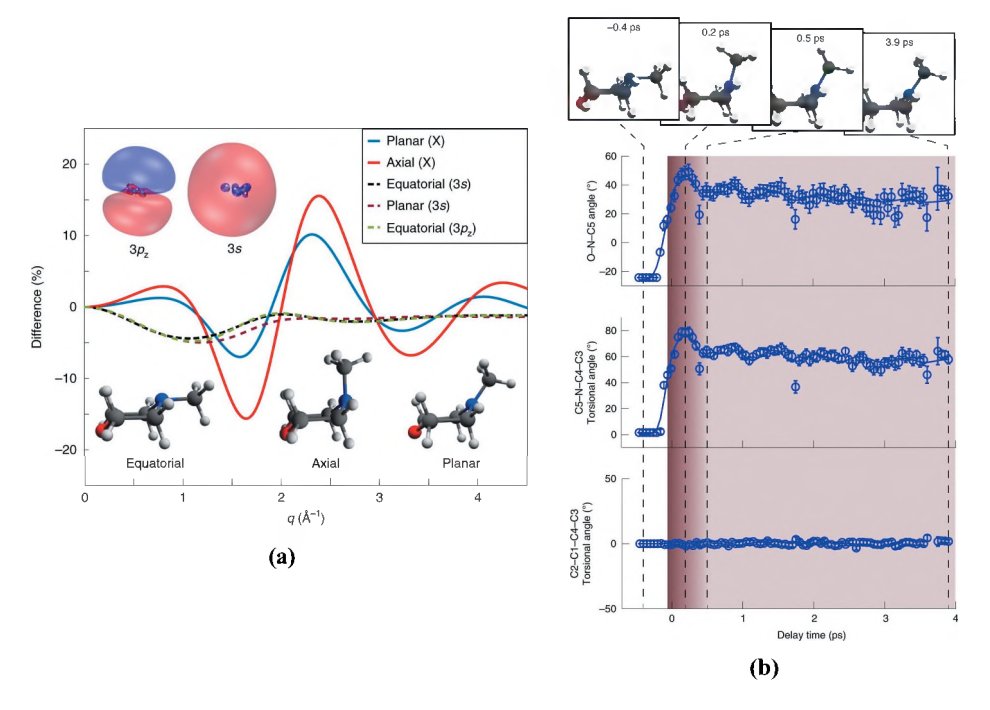


Figure 11. (a) Calculated percent difference scattering signal spectra assuming 100% excitation of the sample. (b) Time dependence of select structural parameters of NMM after Rydberg excitation. Figure from [4].

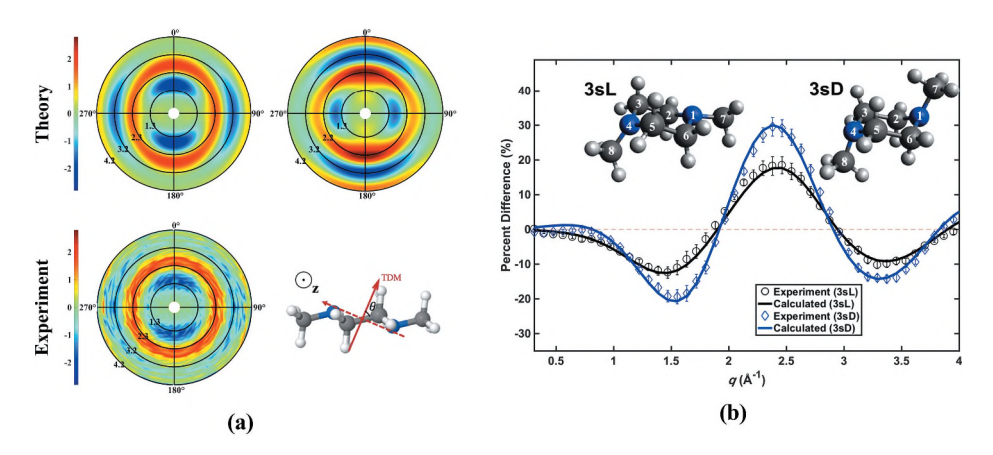


Figure 12. (a) Experimental (bottom left) and theoretical anisotropic contribution to pump-probe signal. The top left pattern depicts the computed transitional dipole moment as shown in solid red arrow, and the top right depicts the scattering signal pattern perpendicular to the transition dipole moment as shown in dotted red arrow. (b) Experimental (marker) and theoretical (solid line) percent difference scattering from isotropic contribution. Two distinct excited state structures were identified; one from charge-localized (black) and charge-delocalized (blue). Figures from [42].

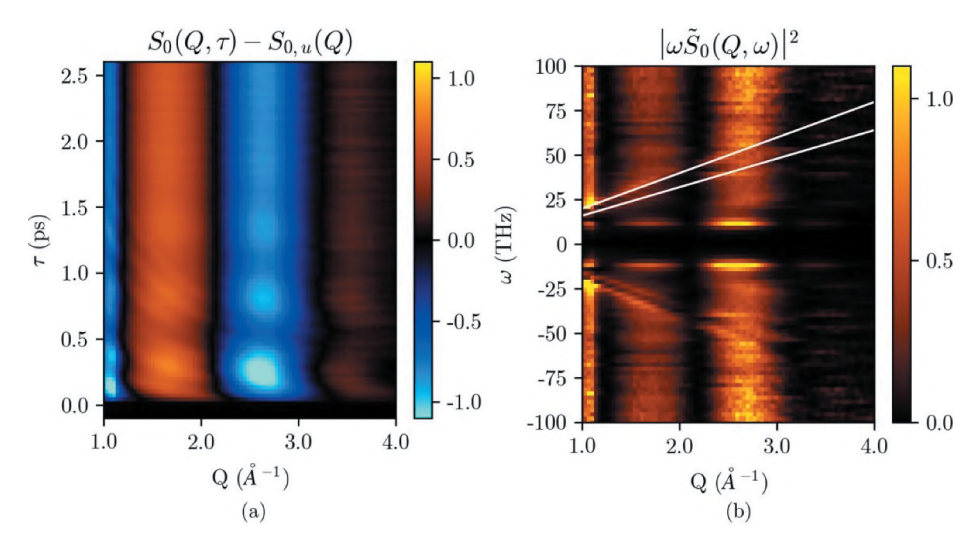


Figure 13. (a) X-ray scattering signal (isotropic component) of molecular iodine pumped at 520 nm (b) Power spectrum of (a) after Fourier transform. The two white lines indicate the two dissociation channels. Figure from [9].

Another method to isolate the specific pathway from multiple simultaneous events was demonstrated by Ware et al. in molecular iodine pumped at 520 nm. They used frequency resolved x-ray scattering (FRXS) and performed a temporal Fourier transform of the time-dependent scattering signal, which was then converted to a power spectrum [9, 11]. From this, the authors were able to identify dissociation from two different states based on the two discrete dissociation velocities as well as the bound B state of iodine, (see in Figure 13). Furthermore, the frequency resolution is $\frac{2\pi}{\tau_{range}}$ compared to the real space spatial resolution of the scattering which is $\frac{2\pi}{q_{max}-q_{min}}$ FRXS is an alternative analysis method that is not limited by the q-range, and thus the FEL radiation available. The analysis takes particular advantage of excellent temporal resolution and data accumulation, so that the data from a large time delay range can be collected to improve the frequency resolution.

Introducing elliptically polarized, linearly chirped laser pulses made aligning of gaseous molecular ensemble possible, thus circumventing the need for rotational averaging. By obtaining the 2D diffraction pattern from 3D aligned planar 2,5-diiodothiophene, Kierspel et al. successfully retrieved the distance between the two iodine atoms in the molecule, which agreed with theoretical calculation within 5%. In principle, the data from an aligned molecule experiment contains 3D structural information of the molecule instead of reducing the information to pair distribution functions or a 2D scattering image [112]. While this study was reported on an I–I distance in a

static molecular frame, with enough improvement in SNR, the setup could be used for time-dependent studies. The upcoming higher repetition rate upgrade of the light sources as well as CW operation would make this experiment significantly more efficient and compatible for time-resolved studies.

Encouraged by the success with prototypical molecules in gas-phase scattering experiments, the natural next step would be to explore chemically complex, larger molecules with subtle structural dynamics. Larger molecular systems benefit from an overall increase in molecular cross sections, but introduce added complexity in understanding of the scattering signal. Theoretical tools are essential in order to anticipate and optimize the experimental parameters accordingly, as well as for understanding the data, which will only become larger in volume and richer in complexity as we head towards higher repetition rate operation [113, 114]. It is common practice to use the independent atom model (IAM) [58], despite its assumption and limitations, as it provides a robust and relatively inexpensive calculation that agrees acceptably with the experiments [3, 56, 115]. An advantage of the IAM is its scalability to larger molecular systems, where higher level calculations become computationally expensive. The accuracy of the IAM should be reviewed with an eve toward replacing it with scattering patterns directly from *ab initio* wavefunctions [116–123].

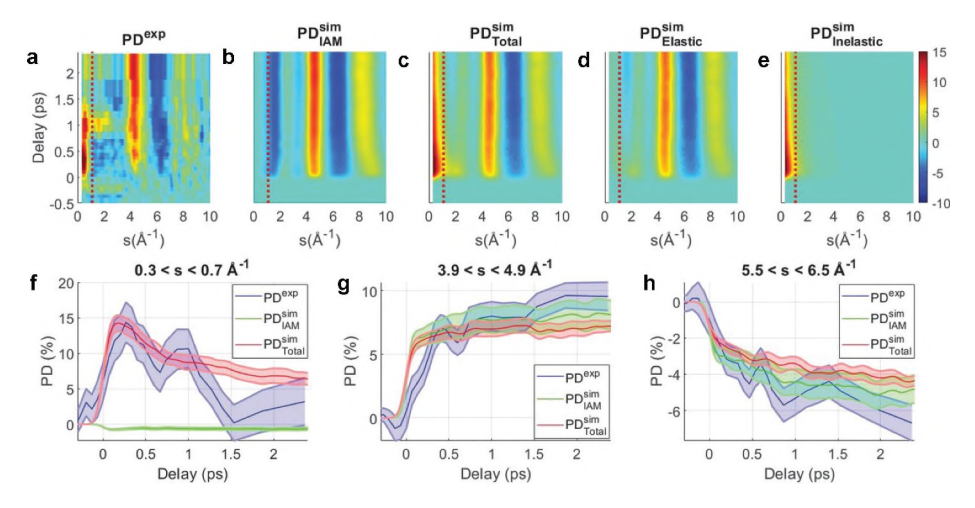


Figure 14. Top row: Experimental percent difference (PD) signal scaled to 9% excitation (a). Simulated PD signal; IAM (b), ab initio electron diffraction (AIED) simulation including both elastic and inelastic component (c), AIED simulation, elastic component-only, and AIED inelastic component-only (d). Lineout of significant features seen in simulations are shown in (F-H). Figures from [23].



6.2 Recent advances in gas-phase UED

The availability of MeV electron pulses overcame previous experimental limits including long pulse duration caused by space-charge effects and velocity mismatch between the electron and the laser pulses as discussed in Section 5. In the experiment by Yang et al., a simultaneous observation of nuclear and electronic dynamics of pyridine after 265 nm pump was achieved with 3.7 MeV electron probe pulses containing ~10⁴ electrons per pulse [23]. The experiment achieved 150 fs FWHM temporal resolution and 0.63 Å^{-1} spatial resolution. From prior studies, the small scattering angle signals $(0.3 < s < 1 \text{ Å}^{-1})$ arise largely from inelastic scattering and therefore probes the excited state population of the molecules. As shown in Figure 14, the dynamics in the small scattering angle region is not captured by the IAM, which ignores chemical bonding, thus concluding that these signals arise from either electron density redistribution (i.e. bond formation) or inelastic effects. This experiment suggests that simultaneous observation and extraction of nuclear and electronic dynamics might possible with UED, and that the method proposed might be adaptable to other molecular systems. If nothing else, the inelastic scattering signal could provide a useful instrument function that helps in deconvoluting the ultrafast dynamics. A study of 1,3-cyclohexadiene by Wolf et al. revealed additional details of this extensively studied electrocyclic reaction [8]. The final product upon 267 nm excitation is 1,3,5-hexatriene (HT) which can be found in three structural isomers separated by 0.2 eV energy barriers on the ground electronic state. This study was the first report of this groundstate isomerization after the initial ring-opening reaction with sub-picosecond resolution. While the experiment was limited to a temporal resolution of 160 fs and thus unable to time-resolve the C-C bond breaking, the sensitivity to the nuclear motions enabled capturing the rotation of the terminal ethylene group in the HT. The experiment also demonstrated the applicability of gas-phase UED to study femtosecond scale molecular dynamics, providing complementary insights to XRS.

The sensitivity to structural evolution was further investigated with the α -phellandrene system, which is a molecule with methyl- and isopropyl-group substituted around five-membered CHD-like ring. There are two possible conformers of the isopropyl group with respect to the methyl group - axial and equatorial - which exist in equilibrium in the ground state. Champenois et al. observed conformer-specific reaction pathways where each conformeric isomer goes through different conical intersections upon excitation, leading to distinct opened-ring products predicted by Woodward-Hoffman rules [25]. They also reported the quantitative agreement with ab initio multiple spawning (AIMS) simulations, which revealed that a significant fraction (52% in axial and 40%

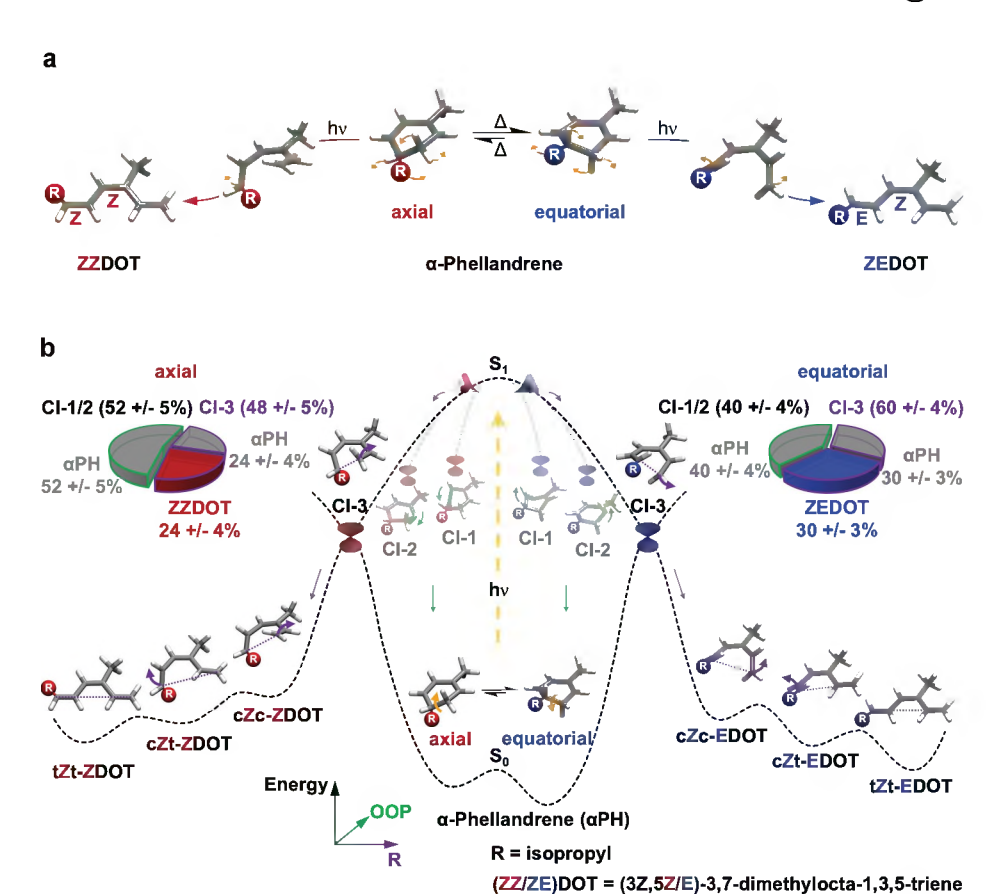


Figure 15. (a) Woodward-Hoffman predicted photoproduct depending on the conformeric isomers. (b) Schematic of the overall reaction based on *ab initio* multiple spawning simulations. The excited molecules undergo conformer-specific conical intersections leading to the respective final product. Figure from [25].

in equatorial) of the ground state molecules do not follow the ringopening pathways, thus aiding a conformer-specific understanding of multiple relaxation processes (Figure 15). The study revealed the considerable effect of the orientation of isopropyl substituents on the quantum yield of the ring-opening reaction, as well as highlighted the sensitivity of MeVUED as an experimental tool that can untangle the chemical reactions with multiple competing pathways.

The temporal resolution has been one of the drawbacks of the MeV-UED technique when compared to XRS, where 30 fs pulses can be delivered to the interaction region. However, ongoing efforts to shorten the pulse duration of MeV-UED instruments are worth noting. There are a number of approaches to reduce the space-charge effects, such as reducing propagation distance, increasing electron energy, and re-compression of electron bunches, although these strategies may require reducing bunch density.

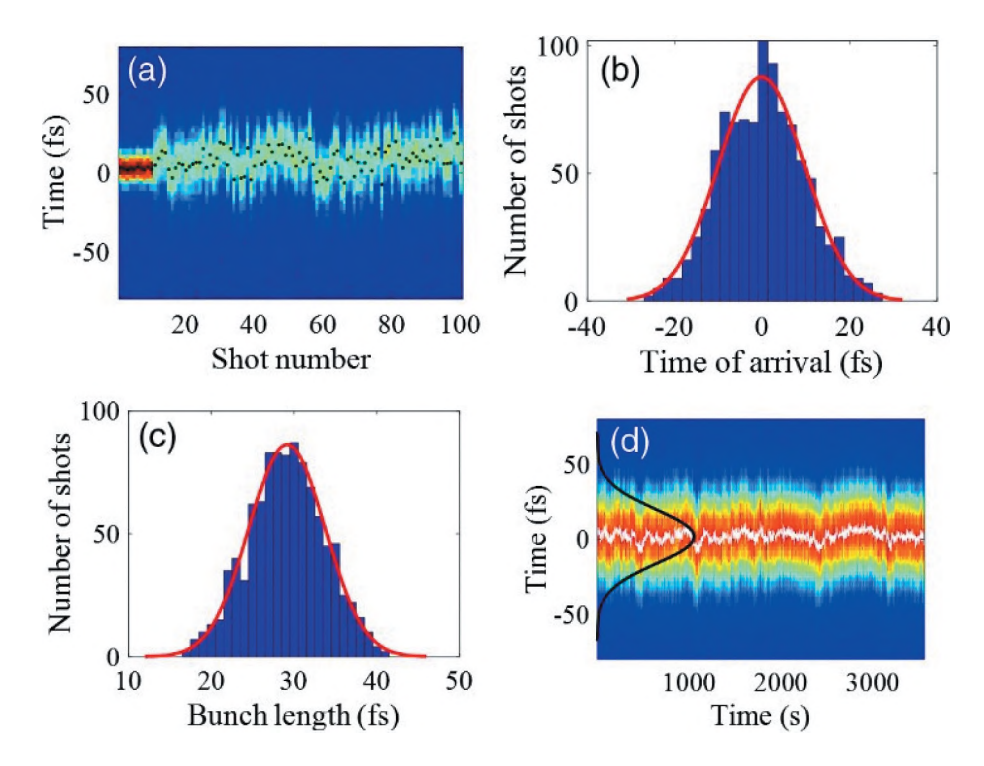


Figure 16. Characterization of DBA compression. (a) Beam temporal profile of 100 consecutive shots wit THz deflector off (first 10 shots) and on. (b) Arrival time statistics. (c) Electron beam pulse duration profile. (d) Stability test of bunch length and arrival time over 1000 shots. Figure from [124].

One such example is demonstrated by Qi et. al., using a double bend achromat (DBA), where an energetically chirped beam undergoes phase space rotation twice such that the bunch tail catches up with the bunch head, resulting in longitudinally compressed pulses [124]. With this method, they were able to achieve 29 fs bunch length with a 20 fC electron beam (Figure 16).

Notably, this is the area where UED will benefit significantly from higher repetition rates, so that low-charge operation with shorter pulse can be achieved, while the loss of scattering signal due to low electron density can be compensated. Recent studies showed that replacing the rf buncher with a laser-driven THz buncher can be used to compress MeV beams, reducing the timing jitter after compression to 70 fs FWHM [125, 126]. Great progress has already been made to increase the time resolution of MeV-UED setups, in particular the one described by Qi et al. Recent gasphase measurements of aligned and isolated CO₂ molecules demonstrated an experimental temporal resolution of approximately 80 fs (FWHM) [127].

| Key ScienceEnablers | CurrentCapability | Anticipated FutureNeed (5 yr) | SolidState | Liq/ GasChem | Stoch/ WDM | Environ. UED |
|--------------------------|--|----------------------------------|------------|-----------------|---------------|-----------------|
| Momentum Resolution | 1.7 nm ⁻¹ | <0.2 nm ⁻¹ | Х | Х | Χ | |
| Temperature Control | 30–800 K | 4–800 K | Х | | Χ | Χ |
| Time Resolution | <150 fs | <50 fs | Χ | Χ | | |
| Probe Size | 100 um | 1 um | Χ | | Χ | |
| Electron Flux | 1-10 fC @ 360 Hz | 30-100 fC @ 1 kHz | Χ | Χ | Χ | Χ |
| Pump laser Wavelength | UV(>240 nm), VIS, NIR, MIR, LWIR, FIR | Extensions to VUV (>160 nm) | | Χ | | Χ |
| High Power Laser | 10 mJ | 100 mJ | | | Χ | |

Table 3. Future (~ 5 year) capability requirements for MeV-UED experiments.

7 Outlook

7.1 Improving gas-phase measurements: What the future holds for MeV and **FEL facilities**

The field of ultrafast gas phase x-ray scattering and electron diffraction has seen tremendous progress in the past decade, and beyond the scope of this review, applications extend to condensed-phase targets that are of interest to the structural biology and material science communities [128-133]. Gas phase scattering will will remain an important sub-field that pushes significant technological advances, as it benefits the most from brighter electron/ light sources, higher repetition rate, greater momentum resolution, and of course overall temporal resolution.

Light sources around the globe are currently undertaking major upgrades to respond to the growing demand for high brilliance, high energy light sources with capabilities for improved spatial and temporal resolution (see Table 3). The European XFEL (Germany) was the first facility to operate with a superconducting accelerator, delivering < 100 fs pulse at 27,000 Hz at 17.5 GeV. The facility is currently undertaking several upgrades including two-color x-ray pump-probe capabilities, frequency mixing, and self-seeding FEL [134].

The European XFEL is not the only light source exploring different seeding mechanism for their FEL. Despite the fact that external seeding is generally only applicable for soft x-rays and thus does not affect the hard x-rays required for gas phase scattering experiments, it is worth noting the extensive ongoing work to optimize FEL pulses. The FLASH 2020+ project at DESY has reported significant improvements in stability and adaptation to high repetition rate through an external seeding mechanism [95, 135].

At SLAC National Accelerator Laboratory, the upgrade of the LCLS comes in two-parts: LCLS-II and LCLS-II-HE. Parts of the former have been available to users since 2020, with nominal pulse durations of 30 fs for hard x-rays up to 25 keV photon energy thanks to all-new variable gap undulators operating at 120 Hz. Starting in early 2023, LCLS-II is anticipated

to come online as the first CW-superconducting XFEL in the world and will feature an unprecedented 1 MHz repetition rate with tunable gap undulators to accommodate soft to hard x-ray energies between 0.25 to 5 keV. This high rep-rate upgrade can potentially enable experiments that previously suffered from low SNR or slow data accumulation, and broaden the application of FELs [136–139]. Further upgrades by way of the LCLS-II-HE project, anticipated in 2026, will extend the hard x-ray reach to well over 10 keV. These facility upgrades are inspiring new scientific endeavors such as singleparticle imaging, which has already succeeded in 3D imaging of virus particles with ~10 nm resolution [140-142]. Lastly, with the recent development of intense, isolated attosecond x-ray pulses [143], it is noteworthy to mention that their application to XRS measurements have only just begun to be explored.

X-ray and electron scattering remain very much complementary techniques that provide the bedrock of structural molecular dynamics. It is anticipated that the combination of the two, or the combination of either with other spectroscopic techniques, will become the standard method for achieving full understanding of dynamic processes in molecular systems. The current trend among light sources for higher repetition rates is in alignment with scientific inquiries that are not limited to gas phase scattering [60, 67, 130, 144]. This will certainly benefit both XRS and UED, but particularly so for the latter, which requires greater data accumulation in order to improve the SNR. While the focus of this review has been on gas phase molecular dynamics, it is worth noting that planned upgrades at MeV-UED facilities, like the one at SLAC, will provide key enabling capabilities for an array of scientific areas within the next 5 years (see Table 3).

The required order of magnitude improvements in reciprocal space (qresolution) and beam size require a reduction in transverse beam emittance (and hence increased beam brightness). Potential approaches to address these issues include electron gun optimization tailored to a UED-specific parameter space (ultra-low charge, high-rep rate), use of alternative cathode materials with lower mean transverse energy (MTE), and operation of normal-conducting cavities at cryogenic temperatures for substantially increased gradients and brightness [145]. Bunch compression techniques using conventional radio frequency structures have succeeded in producing ultralow emittance few-fs beams and represent a significant step towards achieving the high brightness beams needed. However, rf-based acceleration and manipulation suffer from appreciable amplitude and phase jitter depending on the stability of the drive source, causing time-of-arrival litter between the electron beam. The use of a double-bend achromat has been demonstrated as a method to compress the electron beam output from a photocathode rf gun, while at the same time reducing its jitter with respect to the pump laser [146]. Unfortunately, the improvement of time resolution

sacrifices the electron beam transverse brightness since the energy chirp required by this scheme comes from strong space charge effects. Use of THz-driven beam manipulation has been recognized as a promising candidate in the pursuit of few-fs beams with sub-fs arrival time precision, because the inherent timing synchronization of all-optical control enables both bunch compression and reduction of beam timing jitter [125, 147].

With increasing repetition rate, other instrument specific details such as gas sample cell/delivery design, single-shot time stamping, detector technology, and efficient real-time data processing infrastructure must also be upgraded. It should also be noted that as major upgrades of facilities herald a new generation of electron and light sources, it is important to diversify these sources in order to best respond to the range of scientific questions available, to increase accessibility to a wider scientific community that may be unfamiliar with MeV electron and FEL facilities, and to train a future generation of scientists who will continue to utilize and develop the capabilities of these truly world leading facilities.

As the next generation MeV-UED and FEL facilities take shape in the very near future, the field of gas-phase chemistry and molecular dynamics will truly be brighter, faster, and stronger than ever before.

Acknowledgments

The authors are grateful for all the fruitful discussions and strong support we had along the way in drafting this review paper. MPM would especially like to thank Alex Reid, Joel England, and Xiaozhe Shen. Use of the Linac Coherent Light Source (LCLS), MeV-UED, and SLAC National Accelerator Laboratory, is supported by the U.S. Department of Energy, Office of Science, Office of Basic Energy Sciences under Contract # DE-AC02-76SF00515. PMW acknowledges funding by the U.S. Department of Energy, Office of Science, Basic Energy Sciences, Awards # DE-SC0017995 and DE-SC0020276, and the National Science Foundation, Award #CHE-1953839. AK acknowledges funding by the U.S. Department of Energy (Office of Science, Basic Energy Sciences, Award # DE-SC0020276), the EPSRC (grants EP/V049240/1 and EP/V006819/1), the Leverhulme Trust (grant RPG-2020-208), and the Swedish Collegium for Advanced Studies supported by the Erling-Persson Family Foundation and the Knut and Alice Wallenberg Foundation.

Disclosure statement

No potential conflict of interest was reported by the author(s).

Funding

This work was supported by the Engineering and Physical Sciences Research Council [EP/ V049240/1 and EP/V006819/1]; Swedish Collegium for Advanced Study [Erling-Persson Family Foundation, Knut and Alice Wallenberg Foundation]; U.S. Department of Energy, Office of Science, Office of Basic Energy Sciences [DE-AC02-76SF00515,DE-SC0017995,



DE-SC0020276]; US National Science Foundation [CHE-1953839]; The Leverhulme Trust [RPG-2020-208].

References

- [1] Zewail AH. Femtochemistry: atomic-scale dynamics of the chemical bond. J Phys Chem A. 2000 June;104:5660-5694.
- [2] Yong H, Zotev N, Stankus B, et al. Determining orientations of optical transition dipole moments using Ultrafast x-ray scattering. J Phys Chem Lett. 2018 Nov;9:6556– 6562.
- [3] Ruddock JM, Zotev N, Stankus B, et al. Simplicity beneath complexity: counting molecular electrons reveals transients and kinetics of photodissociation reactions. Angew Chem. 2019 May;131:6437-6441.
- [4] Stankus B, Yong H, Zotev N, et al. Ultrafast X-ray scattering reveals vibrational coherence following Rydberg excitation. en. Nat Chem. 2019 Aug;11:716-721. Available from: https://www.nature.com/articles/s41557-019-0291-0(2021)
- [5] Cao J, Wilson KR. Ultrafast X-ray Diffraction Theory. J Phys Chem A. 1998 Nov;102:9523-9530.
- [6] Yong H, Zotev N, Ruddock JM, et al. Observation of the molecular response to light upon photoexcitation. en. Nat Commun. 2020 May;11:2157. Available from: https:// www.nature.com/articles/ s41467-020-15680-4(2021)
- [7] Minitti MP, Budarz J, Kirrander A, et al. Imaging molecular motion: femtosecond x-ray scattering of an electrocyclic chemical reaction. Phys Rev Lett. 2015 June;114:255501.
- [8] Wolf TJA, Sanchez DM, Yang J, et al. The photochemical ring-opening of 1,3cyclohexadiene imaged by ultrafast electron diffraction. en. Nat Chem. 2019 June;11:504-509. Available from: https://www.nature.com/articles/s41557-019-0252-7(2021)
- [9] Ware MR, Glownia JM, Al-Sayyad N, et al. Characterizing dissociative motion in time-resolved x-ray scattering from gas-phase diatomic molecules. Phys Rev A. 2019 Sept;100:033413.
- [10] Natan A, Schori A, Owolabi G, et al. Resolving multiphoton processes with highorder anisotropy ultrafast X-ray scattering, en. Faraday Discuss. 2021 May;228:123-138. Available from: https://pubs.rsc.org/en/content/articlelanding/2021/fd/ d0fd00126k(2022)
- [11] Ware MR, Glownia JM, Natan A, et al. On the limits of observing motion in timeresolved X-ray scattering. Philos Trans R Soc London, Ser A. 2019 May;377:20170477.
- [12] Gelisio L, Scardi P. 100 years of Debye's scattering equation. en. Acta Crystallogr Sect A: Found Adv. 2016 Nov;72:608-620. Available from: http://scripts.iucr.org/cgi-bin/ paper?ib5049(2021)
- [13] Mark H, Wierl R. Über Elektronenbeugung am einzelnen Molekül. de. Naturwissenschaften. 1930 Feb;18:205
- [14] Hargittai I, Hargittai M, editors. Stereochemical applications of gas-phase electron: diffraction, Part A. New York: VCH; 1988 Oct.
- [15] Mourou G, Williamson S. Picosecond electron diffraction. Appl Phys Lett. 1982 July;41(41):44–45.
- [16] Ischenko AA, Golubkov VV, Spiridonov VP, et al. A stroboscopical gas-electron diffraction method for the investigation of short-lived molecular species. en. Appl Phys B. 1983 Nov;32:161-163.



- [17] Ewbank JD, Schäfer L, Paul DW, et al. Real-time data acquisition for gas electron diffraction. Rev Sci Instrum. 1984 Oct;55:1598-1603. Available from: https://aip. scitation.org/doi/abs/10.1063/1.1137624(2021)
- [18] Williamson JC, Dantus M, Kim SB, et al. Ultrafast diffraction and molecular structure. en. Chem Phys Lett. 1992 Aug;196:529-534. Available from: https://www.sciencedir ect.com/science/article/pii/000926149285988M(2021)
- [19] Weber PM, Carpenter SD, Lucza T. Reflectron design for femtosecond electron guns. In Time-resolved electron and x-ray diffraction, Vol. 2521, SPIE; 1995 Sept. p.23–30. Available from: https://www.spiedigitallibrary.org/conference-proceedings-of-spie/ 2521/0000/Reflectron-design-for-femtosecond-electron-guns/10.1117/12.218364.full (2021).
- [20] Dudek RC, Weber PM. Ultrafast diffraction imaging of the electrocyclic ring-opening reaction of 1,3-Cyclohexadiene. J Phys Chem A. 2001 May;105:4167-4171. DOI:10. 1021/jp010122t(2021).
- [21] Siwick BJ, Dwyer JR, Jordan RE, et al. An atomic-level view of melting using femtosecond electron diffraction. eng. Science. 2003 Nov;302:1382-1385.
- [22] Cao J, Hao Z, Park H, et al. Femtosecond electron diffraction for direct measurement of ultrafast atomic motions. Appl Phys Lett. 2003 Aug;83:1044-1046. Available from: https://aip.scitation.org/doi/10.1063/1.1593831(2022)
- [23] Yang J, Zhu X, F. Nunes JP, et al. Simultaneous observation of nuclear and electronic dynamics by ultrafast electron diffraction. en. Science. 2020 May;368:885-889. Available from: https://science. sciencemag.org/content/368/6493/885(2021)
- [24] Lin M-F, Singh N, Liang S, et al. Imaging the short-lived hydroxyl-hydronium pair in ionized liquid water. Science. 2021 Oct;374:92-95.
- [25] Champenois EG, Sanchez DM, Yang J, et al. Conformer-specific photochemistry imaged in real space and time. Science. 2021 Oct;374:178-182.
- [26] Rose-Petruck C, Jimenez R, Guo T, et al. Picosecond-milliangström lattice dynamics measured by ultrafast X-ray diffraction. en. Nature. 1999 Mar;398:310-312. Available from: https://www.nature.com/articles/18631 (2021)
- [27] Rischel C, Rousse A, Uschmann I. Femtosecond time-resolved X-ray diffraction from laser-heated organic films. Nature. Dec 1997;390:490.
- [28] Lindenberg AM, Kang I, Johnson SL, et al. Time-resolved x-ray diffraction from coherent phonons during a laser-induced phase transition. Phys Rev Lett. 2000 Jan;84:111-114.
- [29] Siders CW, Cavalleri A, Sokolowski-Tinten K, et al. Detection of nonthermal melting by ultrafast x-ray diffraction. Science. 1999 Nov;286:1340-1342.
- [30] Madey JMJ. Stimulated emission of bremsstrahlung in a periodic magnetic field. J Appl Phys. 1971 Apr;42:1906–1913. Available from: https://aip.scitation.org/doi/10. 1063/1.1660466(2022)
- [31] Kroll N, Morton P, Rosenbluth M. Free-electron lasers with variable parameter wigglers. IEEE J Quantum Electron. 1981 Aug;17(8):1436–1468.
- [32] Kondratenko AM, Saldin EL. Generation of coherent radiation by a relativistic electron beam in an ondulator. Engl Part Accel. Aug 1980;10:3-4. Available from: https://www.osti.gov/etdeweb/biblio/6018038(2021)
- [33] Georgescu I. The first decade of XFELs. en. Nat Rev Phys. 2020 Jul;2:345.
- [34] Ayvazyan V, Baboi N, Bähr J, et al. First operation of a free-electron laser generating GW power radiation at 32 nm wavelength. en. Eur Phys J D. 2006 Feb;37:297–303.
- [35] Pile D. First light from SACLA. en. Nat Photonics. 2011; 5. Aug. 456–457.
- [36] Allaria E, Appio R, Badano L, et al. Highly coherent and stable pulses from the Fermi seeded free-electron laser in the extreme ultraviolet. en. Nat Photonics. 2012



- Oct;6:699-704. Available from: https://www.nature.com/articles/nphoton.2012.233
- [37] Stankus B, Yong H, Ruddock J, et al. Advances in ultrafast gas-phase x-ray scattering. en. J Phys B. 2020Nov;53:234004.
- [38] Ma L, Yong H, Geiser JD, et al. Ultrafast x-ray and electron scattering of free molecules: a comparative evaluation. Struct Dyn. 2020 May;7:034102.
- [39] Stefanou M, Saita K, Shalashilin DV, et al. Comparison of ultrafast electron and X-ray diffraction - a computational study, en. Chem Phys Lett. 2017;683:300-305. Available from: https://www.sciencedirect.com/science/article/pii/S0009261417302191(2022)
- [40] Ben-Nun M, Martínez TJ, Weber PM, et al. Direct imaging of excited electronic states using diffraction techniques: theoretical considerations. en. Chem Phys Lett. 1996 Nov;262:405–414. Available from: https://www.sciencedirect.com/science/article/pii/ 0009261496011086(2022)
- [41] Kirrander A. X-ray diffraction assisted spectroscopy of Rydberg states. J Chem Phys. 2012;137:154310.
- [42] Yong H, Xu X, Ruddock JM, et al. Ultrafast X-ray scattering offers a structural view of excited-state charge transfer. Proc Nat Acad Sci. 2021 May;118:e2021714118.
- [43] Hartmann N, Helml W, Galler A, et al. Sub-femtosecond precision measurement of relative X-ray arrival time for free-electron lasers. en. Nat Photonics. 2014 Sept;8:706-709. https://www.nature.com/articles/nphoton.2014.164 (2022)
- [44] Travers JC, Grigorova TF, Brahms C, et al. High-energy pulse self-compression and ultraviolet generation through soliton dynamics in hollow capillary fibres. Nat Photonics. 2019 Aug;13:547-554.
- [45] Beutler M, Ghotbi M, Noack F. Generation of intense sub-20-fs vacuum ultraviolet pulses compressed by material dispersion. EN. Opt Lett. 2011; 36. Oct. 3726–3728.
- [46] Weathersby SP, Brown G, Centurion M, et al. Mega-electron-volt ultrafast electron diffraction at SLAC national accelerator laboratory. Rev Sci Instrum. 2015 July;86:073702.
- [47] Tao Z, Zhang H, Duxbury PM, et al. Space charge effects in ultrafast electron diffraction and imaging. J Appl Phys. 2012;111:044316.
- [48] Van Oudheusden T, de Jong EF, van der Geer SB, et al. Electron source concept for single-shot sub-100 fs electron diffraction in the 100 keV range. J Appl Phys. 2007 Nov;102:093501.
- [49] Baum P, Zewail AH. Breaking resolution limits in ultrafast electron diffraction and microscopy. Proc Nat Acad Sci. Oct 2006;103:16105-16110. Available from: https:// www.pnas.org/doi/full/10.1073/pnas.0607451103(2022)
- [50] Xiong Y, Wilkin KJ, Centurion M. High-resolution movies of molecular rotational dynamics captured with ultrafast electron diffraction. Phys Rev Res. Oct 2020;2:043064. Available from: https://link.aps.org/doi/10.1103/PhysRevResearch.2. 043064(2022)
- [51] Hastings JB, Rudakov FM, Dowell DH, et al. Ultrafast time-resolved electron diffraction with megavolt electron beams. Appl Phys Lett. 2006 Oct;89:184109. Available from: https://aip.scitation.org/doi/full/10.1063/1.2372697(2022)
- [52] Li R, Tang C, Du Y, et al. Experimental demonstration of high quality MeV ultrafast electron diffraction. Rev Sci Instrum. 2009 Aug;80:083303. Available from: https://aip. scitation.org/doi/full/10.1063/1.3194047(2021)
- [53] Shen X, Nunes JPF, Yang J, et al. Femtosecond gas-phase mega-electron-volt ultrafast electron diffraction. Struct Dyn. 2019 Sept;6:054305.
- [54] Maxson J, Cesar D, Calmasini G, et al. Direct measurement of sub-10 fs relativistic electron beams with ultralow emittance. Phys Rev Lett. 2017 Apr;118:154802.



- [55] Blaschke JP, Brewster AS, Paley DW, et al. Real-time XFEL data analysis at SLAC and NERSC: a trial run of nascent exascale experimental data analysis. eng. ArXiv. 2021;2106:11469v2.
- [56] Yong H, Moreno Carrascosa A, Ma L, et al. Determination of excited state molecular structures from time-resolved gas-phase X-ray scattering. en. Faraday Discuss. 2021 May;228:104-122. Available from: https://pubs.rsc.org/en/content/articlelanding/ 2021/fd/d0fd00118j(2022)
- [57] Yong H, Cavaletto SM, Mukamel S. Ultrafast valence-electron dynamics in oxazole monitored by x-ray diffraction following a stimulated x-ray Raman excitation. J Phys Chem Lett. 2021Oct;12:9800-9806.
- [58] Kirrander A, Weber PM. Fundamental limits on spatial resolution in ultrafast x-ray diffraction. en. Appl Sci. 2017 June;7:534.
- [59] Hensley CJ, Yang J, Centurion M. Imaging of isolated molecules with ultrafast electron pulses. Phys Rev Lett. 2012 Sept;109:133202.
- [60] Ischenko AA, Weber PM, Miller RJD. Capturing chemistry in action with electrons: realization of atomically resolved reaction dynamics. Chem Rev. 2017 Aug;117:11066-11124.
- [61] Schoenlein RW. LCLS-II high energy (LCLS-II-HE): a transformative X-ray laser for science English. Tech. rep. SLAC-R-1143. Menlo Park (CA):SLAC National Accelerator Lab; Jan. 2016. Available from: https://www.osti.gov/biblio/1634206 (2022).
- [62] Hemsing E, Stupakov G, Xiang D, et al. Beam by design: laser manipulation of electrons in modern accelerators. Rev Mod Phys. 2014 July;86:897-941.
- [63] Seddon EA, Clarke JA, Dunning DJ, et al. Short-wavelength free-electron laser sources and science: a review. en. Rep Prog Phys. 2017Oct;80:115901.
- [64] Attwood D, Sakdinawat A. X-rays and extreme ultraviolet radiation: principles and applications. 2nd ed. Cambridge: Cambridge University Press; 2017. Available from: https://www.cambridge.org/core/books/ xrays-and-extreme-ultraviolet-radiation/ 8909199B5EDEDE542FCD1EBDD829D47C (2022)
- [65] Yurkov M, Schneidmiller E. Coherence Limits of X-ray FEL Radiation en. Geneva (SL): JACOW; 2018 Feb, p. 5-8. Available from: https://accelconf.web.cern.ch/ fel2017/doi/JACoW-FEL2017-MOBA02.html(2022)
- [66] Feng C, Deng H-X. Review of fully coherent free-electron lasers. en. Nucl Sci Tech. 2018 Sept;29:160.
- [67] Schoenlein R, Elsaesser T, Holldack K, et al. Recent advances in ultrafast X-ray sources. Philos Trans R Soc A Math Phys Eng Sci. 2019 May;377(2145):20180384.
- [68] Nunes JPF, Ledbetter K, Lin M, et al. Liquid-phase mega-electron-volt ultrafast electron diffraction. Struct Dyn. 2020 Mar;7:024301.
- [69] Li RK, Musumeci P, Bender HA, et al. Imaging single electrons to enable the generation of ultrashort beams for single-shot femtosecond relativistic electron diffraction. J Appl Phys. 2011 Oct;110(7): 074512.
- [70] Murooka Y, Naruse N, Sakakihara S, et al. Transmission-electron diffraction by MeV electron pulses. Appl Phys Lett. 2011 June;98:251903. Available from: https://aip. scitation.org/doi/10.1063/1.3602314(2022)
- [71] Zhu P, Zhu Y, Hidaka Y, et al. Femtosecond time-resolved MeV electron diffraction. en. New J Phys. 2015 June;17:063004.
- [72] Bonifacio R, Pellegrini C, Narducci LM. Collective instabilities and high-gain regime in a free electron laser. en. Opt Commun. July 1984;50:373-378.



- [73] Bonifacio R, De Salvo L, Pierini P, et al. Spectrum, temporal structure, and fluctuations in a high-gain free- electron laser starting from noise. Phys Rev Lett. 1994 July;73:70-73.
- [74] Reiche S, Musumeci P, Pellegrini C, et al. Development of ultra-short pulse, single coherent spike for SASE X-ray FELs. en. Nucl Instrum Methods Phys Res, Sect A 2007. 2008 Aug;593:45-48.
- [75] Scheinker A, Bohler D, Tomin S, et al. Model-independent tuning for maximizing free electron laser pulse energy. Phys Rev Accel Beams. 2019 Aug;22:082802.
- [76] Emma P, Bane K, Cornacchia M, et al. Femtosecond and subfemtosecond x-ray pulses from a self-amplified spontaneous-emission-based free-electron laser. Phys Rev Lett. 2004 Feb;92:074801.
- [77] Prat E, Bettoni S, Reiche S. Enhanced X-ray free-electron-laser performance from tilted electron beams, en. Nuclear instruments and methods in physics research section a: accelerators, spectrometers, detectors and associated equipment. Phys Appl High Brightness Beams. Sept. 2017 2016;865:1-8. Available from: https:// www.sciencedirect.com/science/article/pii/S0168900216307057(2022)
- [78] Amann J, Berg W, Blank V, et al. Demonstration of self-seeding in a hard-X-ray freeelectron laser. en. Nat Photonics. 2012 Oct;6:693-698. https://www.nature.com/arti cles/nphoton.2012.180(2022)
- [79] Jamison S. X-ray FEL shines brightly. en. Nat Photonics. 2010 Sept;4:589–591.
- [80] Ratner D, Abela R, Amann J, et al. Experimental demonstration of a soft x-ray selfseeded free-electron laser. Phys Rev Lett. 2015 Feb;114:054801.
- [81] Hirata K, Shinzawa-Itoh K, Yano N, et al. Determination of damage-free crystal structure of an X-ray-sensitive protein using an XFEL. en. Nat Methods. 2014 July;11:734-736. Available from: https://www.nature.com/articles/nmeth.2962(2022)
- [82] Cox N, Pantazis DA, Lubitz W. Current understanding of the mechanism of water oxidation in photosystem II and its relation to XFEL data. Annu Rev Biochem. 2020;89:795-820.
- [83] Hosseinizadeh A, Breckwoldt N, Fung R, et al. Few-fs resolution of a photoactive protein traversing a conical intersection. Nature. 2021 Nov;599:697-701. Available from: https://www.nature.com/articles/s41586-021-04050-9(2022)
- [84] Witte BBL, Fletcher L, Galtier E, et al. Warm dense matter demonstrating non-Drude conductivity from observations of nonlinear plasmon damping. Phys Rev Lett. 2017 May;118:225001.
- [85] Gamboa EJ, Fletcher LB, Lee HJ, et al. Single-shot measurements of plasmons in compressed diamond with an x-ray laser. Physics of Plasmas. 2015 May;22:056319. Available from: https://aip.scitation.org/doi/full/10.1063/1.4921407(2022)
- [86] Fletcher LB, Lee HJ, Döppner T, et al. Ultrabright X-ray laser scattering for dynamic warm dense matter physics. en. Nat Photonics. 2015 Apr;9:274-279. Available from: https://www.nature.com/articles/nphoton.2015.41(2022)
- [87] Wu J, Huang X, Raubenheimer T, et al. Recent on-line taper optimization on LCLS en. Geneva (Switzerland):JACOW; 2018 Feb. pp.229-234. Available from: https:// accelconf.web.cern.ch/fel2017/doi/JACoW-FEL2017-TUB04.html(2022).
- [88] Schneidmiller EA, Faatz B, Kuhlmann M, et al. First operation of a harmonic lasing self-seeded free electron laser. Phys Rev Accel Beams. 2017 Feb;20:020705.
- [89] Faatz B, Braune M, Hensler O, et al. The FLASH facility: advanced options for FLASH2 and future perspectives. en. Appl Sci. 2017 Nov;7:1114. Available from: https://www.mdpi.com/2076-3417/7/11/1114 (2022)
- [90] Benson S, Gubeli J, Neil G. An experimental study of an FEL oscillator with a linear taper. Litvinenko VN, Wu YK eds. Nucl Instrum Methods A. 2001;475:276-280.



- [91] Saldin EL, Schneidmiller EA, Yurkov MV. Self-amplified spontaneous emission FEL with energy-chirped electron beam and its application for generation of attosecond xray pulses. Phys Rev Spec Top Accel Beams. May 2006;9:050702. Available from: https://link.aps.org/doi/10.1103/PhysRevSTAB.9.050702 (2022)
- [92] Coffee RN, Cryan JP, Duris J, et al. Development of ultrafast capabilities for X-ray free-electron lasers at the linac coherent light source. Philos Trans R Soc A Math Phys Eng Sci. 2019 May;377(20180386). Available from: https://royalsocietypublishing.org/ doi/10.1098/rsta.2018.0386(2021)
- [93] Huang N, Deng H, Liu B, et al. Features and futures of X-ray free-electron lasers. en. Innovation, 2021 May;2:100097.
- [94] Yu L-H, Babzien M, Ben-Zvi I, et al. High-gain harmonic-generation free-electron laser. Science. 2000 Aug;289:932-934.
- [95] Allaria E, Hartl MB, Kazemi M, et al. FLASH2020+: the new high repetition rate coherent soft x-ray facility EN. In: Conference on Lasers and Electro-Optics (2021), paper FTu2O.5. Optical Society of America; May 2021, p.FTu2O.5. Available from: https://www.osapublishing.org/abstract.cfm?uri=CLEO_QELS-2021-FTu2O.5(2022).
- [96] Paraskaki G, Allaria E, Yurkov M, et al. Options for high-repetition-rate seeded FEL in EUV and X-ray optics, sources, and instrumentation 11776. SPIE; Apr. 2021, 90-99. Available from: https://www.spiedigitallibrary.org/conference-proceedings-ofspie/11776/117760M/Options-for-high-repetition-rate-seeded-FEL/10.1117/12. 2589693.full(2022)
- [97] Feng C, Deng H, Zhang M, et al. Coherent extreme ultraviolet free-electron laser with echo-enabled harmonic generation. Phys Rev Accel Beams. 2019 May;22:050703.
- [98] Giannessi L. en. in synchrotron light sources and free-electron lasers: accelerator physics. In: Jaeschke E, et al., editor. Instrumentation and science applications. Cham: Springer International Publishing; 2014. p. 1-27. DOI:10.1007/978-3-319-04507-8_3-1(2022).
- [99] Reiche S. 4th Int Part Accel Conf. Shanghai, China; 2013; p. 2063- 2067. ISBN: 978-3-95450-122-9.
- [100] Pop M, Allaria E, Curbis F, et al. Single-shot transverse coherence in seeded and unseeded free-electron lasers: a comparison. Phys Rev Accel Beams. 2022 Apr;25:040701.
- [101] Glownia JM, Natan A, Cryan J, et al. Self-referenced coherent diffraction X-ray movie of Ångstrom- and femtosecond-scale atomic motion. Phys Rev Lett. 2016 Oct;117:153003.
- [102] Yang J, Guehr M, Shen X, et al. Diffractive imaging of coherent nuclear motion in isolated molecules. Phys Rev Lett. 2016 Oct;117:153002.
- [103] Budarz JM, Minitti MP, Cofer-Shabica DV, et al. Observation of femtosecond molecular dynamics via pump-probe gas phase x-ray scattering. en. J Phys B. 2016 Jan;49:034001.
- [104] Wolter B, Pullen MG, Le A-T, et al. Ultrafast electron diffraction imaging of bond breaking in di-ionized acetylene. en. Science. 2016 Oct;354:308-312, 1095-9203.
- [105] Zong A, Dolgirev PE, Kogar A, et al. Role of equilibrium fluctuations in light-induced order. Phys Rev Lett. 2021 Nov;127:227401.
- [106] Sood A, Shen X, Shi Y, et al. Universal phase dynamics in VO 2 switches revealed by ultrafast operando diffraction. Science. 2021 July;373:352-355.
- [107] Boll R, Schäfer JM, Richard B, et al. X-ray multiphoton-induced Coulomb explosion images complex single molecules. en. Nat Phys. 2022 Apr;18:423-428. Available from: https://www.nature.com/articles/ s41567-022-01507-0 (2022)



- [108] Turenne D, Yaroslavtsev A, Wang X, et al. Nonequilibrium sub-10 nm spin-wave soliton formation in FePt nanoparticles. Sci Adv. 2022 Apr;8:eabn0523.
- [109] Padmanabhan H, Poore M, Kim PK, et al. Interlayer magnetophononic coupling in MnBi2Te4, en. Nat Commun. 2022 Apr;13:1929. Available from https://www.nature. com/articles/s41467- 022-29545-5 (2022)
- [110] Zhang Y, Jónsson H, Weber PM, et al. Coherence in nonradiative transitions: internal conversion in Rydbergexcited N-methyl and N-ethyl morpholine. Phys Chem Chem Phys. 2017;19:26403.
- [111] Deb S, Cheng X, Weber PM. Structural dynamics and charge transfer in electronically excited N,N-dimethylpiperazine. J Phys Chem Lett. 2013Aug;4:2780-2784.
- [112] Kierspel T, Morgan A, Wiese J, et al. X-ray diffractive imaging of controlled gas-phase molecules: toward imaging of dynamics in the molecular frame. J Chem Phys. 2020 Feb;152:084307.
- [113] Kirrander A, Saita K, Shalashilin DV. Ultrafast X-ray scattering from molecules. J Chem Theory Comput. 2016 Mar;12:957-967.
- [114] Simmermacher M, Henriksen NE, Møller KB, et al. Electronic coherence in ultrafast X-ray scattering from molecular wave packets. Phys Rev Lett. 2019 Feb;122:073003.
- [115] Ruddock JM, Yong H, Stankus B, et al. A deep UV trigger for ground-state ringopening dynamics of 1,3-cyclohexadiene. en. Sci Adv. 2019 Sept;5:eaax6625. Available from: https://advances.sciencemag.org/content/5/9/eaax6625(2021)
- [116] Northey T, Zotev N, Kirrander A. Ab initio calculation of molecular diffraction. J Chem Theory Comput. 2014 Nov; 10: 4911-4920.
- [117] Northey T, Moreno Carrascosa A, Schäfer S, et al. Elastic X-ray scattering from stateselected molecules. J Chem Phys. 2016 Oct;145:154304.
- [118] Carrascosa AM, Northey T, Kirrander A. Imaging rotations and vibrations in polyatomic molecules with X-ray scattering. en. Phys Chem Chem Phys. Mar 2017;19:7853-7863.
- [119] Carrascosa AM, Kirrander A. Ab initio calculation of inelastic scattering. en. Phys Chem Chem Phys. Aug 2017;19:19545-19553.
- [120] Abela R, Alarcon A, Alex J, et al. The SwissFEL soft X-ray free-electron laser beamline: athos. en. J Synchrotron Radiat. 2019 July;26:1073-1084. Available from: https:// journals.iucr.org/s/issues/2019/04/00/yi5074/(2022)
- [121] Moreno Carrascosa A, Yong H, Crittenden DL, et al. Ab initio calculation of total X-ray scattering from molecules. J Chem Theory Comput. 2019 May;15:2836–2846. Available from: https://doi.org/10.1021/acs.jctc.9b00056(2022)
- [122] Zotev N, Moreno Carrascosa A, Simmermacher M, et al. Excited electronic states in total isotropic scattering from molecules. J Chem Theory Comput. 2020 Apr;16:2594–
- [123] Parrish RM, Martínez TJ. Ab initio computation of rotationally-averaged pumpprobe X-ray and electron diffraction signals. J Chem Theory Comput. 2019 Mar;15:1523-1537.
- [124] Qi F, Ma Z, Zhao L, et al. Breaking 50 femtosecond resolution barrier in MeV ultrafast electron diffraction with a double bend achromat compressor. Phys Rev Lett. 2020 Mar;124(13): 134803.
- [125] Snively EC, Othman M, Kozina M, et al. Femtosecond compression dynamics and timing jitter suppression in a THz-driven electron bunch compressor. Phys Rev Lett. 2020 Feb;124:054801.
- [126] Zhao L, Tang H, Lu C, et al. Femtosecond relativistic electron beam with reduced timing jitter from THz driven beam compression. Phys Rev Lett. 2020 Feb;124:054802.



- [127] Ma Z, Zou X, Zhao L, et al. Ultrafast isolated molecule imaging without crystallization. Proc Nat Acad Sci. 2022 Apr;119:e2122793119.
- [128] Zettergren H, Domaracka A, Schlathölter T, et al. Roadmap on dynamics of molecules and clusters in the gas phase. en. Eur Phys J D. May 2021;75:152.
- [129] Orville AM. Recent results in time resolved serial femtosecond crystallography at XFELs. en. Curr Opin Struct Biol. 2020 Dec;65:193-208. Available from: https://www. sciencedirect.com/science/article/pii/S0959440X20301482 (2022)
- [130] Ueda K, Sokell E, Schippers S, et al. Roadmap on photonic, electronic and atomic collision physics: I. Light-matter interaction. en. J Phys B. 2021 Aug;52:171001.
- [131] Chapman HN. X-ray free-electron lasers for the structure and dynamics of macromolecules. Annu Rev Biochem. 2022;88:35-58.
- [132] Liebschner D, Afonine PV, Baker ML, et al. Macromolecular structure determination using X-rays, neutrons and electrons: recent developments in Phenix. Acta Crystallograph Sect D: Struct Biol. 2019 Oct;75:861-877. Available from: https:// journals.iucr.org/d/issues/2019/10/00/di5033/(2022)
- [133] Boutet S, Lomb L, Williams GJ, et al. High-resolution protein structure determination by serial femtosecond crystallography. Science. 2012 July;337:362-364.
- [134] Geloni GA. Development of advanced FEL techniques at the European XFEL in EUV and X-ray Optics, Sources, and Instrumentation 11776. SPIE; 2021 Apr, p.117760N. Available from: https:// www .spiedigitallibrary.org/conference- proceedings- ofspie/11776/117760N/Development- of- advanced- FEL- techniques- at- the-European- XFEL/10.1117/12.2593118.full(2022).
- [135] Ackermann S, Faatz B, Grattoni V, et al. Novel method for the generation of stable radiation from free-electron lasers at high repetition rates. Phys Rev Accel Beams. 2020 July;23:071302.
- [136] Galayda J. The LCLS-II: a High Power Upgrade to the LCLS. en. Proceedings of the 9th Int. Particle Accelerator Conf. Vancouver, BC, Canada: IPAC2018; 2018. Accessed 06 25 2021. http://jacow.org/ipac2018/doi/JACoW-IPAC2018-MOYGB2. html
- [137] Halavanau A, Decker F-J, Emma C, et al. Very high brightness and power LCLS-II hard X-ray pulses. en. J Synchrotron Radiat. 2019 May;26:635-646. Available from: https://journals.iucr.org/s/issues/2019/03/00/co5121/(2022)
- [138] Decking W, Abeghyan S, Abramian P, et al. A MHz-repetition-rate hard X-ray freeelectron laser driven by a superconducting linear accelerator. en. Nat Photonics. 2020 June;14:391-397.
- [139] LCLS Parameters. 2017 Feb. Available from: https://lcls.slac.stanford.edu/parameters (2022)
- [140] Sun Z, Fan J, Li H, et al. Current status of single particle imaging with X-ray lasers. en. Appl Sci. 2018 Jan;8:132.
- [141] Aquila A, Barty A, Bostedt C, et al. The linac coherent light source single particle imaging road map. Struct Dyn. 2015 July;2:041701.
- [142] Emma C, et al. High efficiency, multiterawatt x-ray free electron lasers. Phys Rev Accel Beams. 2016;19:020705. Available from: https://link.aps.org/doi/10.1103/ PhysRevAccelBeams.19.020705(2022)
- [143] Duris J, Li S, Driver T, et al. Tunable isolated attosecond X-ray pulses with gigawatt peak power from a free-electron laser. en. Nat Photonics. 2020 Jan;14:30-36. Available from: https://www.nature.com/articles/s41566-019-0549-5(2022)
- [144] Lindroth E, Calegari F, Young L, et al. Challenges and opportunities in attosecond and XFEL science. en. Nat Rev Phys. 2019 Feb;1:107-111. Available from: https:// www.nature.com/articles/s42254- 019-0023-9(2022)



- [145] Cahill AD, Fukasawa A, Pakter R, et al. RF design for the TOPGUN photogun: a cryogenic normal conducting copper electron gun. en. Nucl Instrum Methods Phys Res Sect A. 2017 Sept;865:105–108.
- [146] Kim HW, Vinokurov NA, Baek IH, et al. Towards jitter-free ultrafast electron diffraction technology. en. Nat Photonics. 2022 Apr;14(245-249). Available from: https://www.nature.com/articles/s41566-019-0566-4
- [147] Li RK, Hoffmann M, Nanni E, et al. Terahertz-based subfemtosecond metrology of relativistic electron beams. Phys Rev Accel Beams. 2019 Jan;22:012803.